THE UNIVERSITY OF CALGARY

Hairs, Textures, and Shades: Improving the Realism of Plant Models Generated with L-Systems

by

Martin Fuhrer

A THESIS
SUBMITTED TO THE FACULTY OF GRADUATE STUDIES
IN PARTIAL FULFILLMENT OF THE REQUIREMENTS FOR THE
DEGREE OF MASTER OF SCIENCE

DEPARTMENT OF COMPUTER SCIENCE

CALGARY, ALBERTA

August, 2005

THE UNIVERSITY OF CALGARY

FACULTY OF GRADUATE STUDIES

The undersigned certify that they have read, and recommend to the Faculty of Graduate Studies for acceptance, a thesis entitled "Hairs, Textures, and Shades: Improving the Realism of Plant Models Generated with L-Systems" submitted by Martin Fuhrer in partial fulfillment of the requirements for the degree of Master of Science.

Supervisor,
Dr. Przemyslaw Prusinkiewicz
Department of Computer Science

Co-supervisor,
Dr. Brian Wyvill
Department of Computer Science

Dr. Mario Costa Sousa
Department of Computer Science

Gerald Hushlak
Department of Art

Date

Abstract

High-quality, realistic visualization of plant models is a long-standing goal in computer graphics. Plants are often modeled using L-systems. Strings of symbols generated by the L-systems may be interpreted graphically as drawing commands to a rendering system. In this research, techniques for improving the appearance of plants generated from L-systems are proposed. A method of incorporating dynamic material specifications in L-system strings is presented, along with shading and lighting considerations for leaves and petals. Texture mapping of generalized cylinders is revisited in order to properly fit leaf and petal textures onto surfaces, and procedural methods for generating venation patterns and translucent rims on these surfaces are introduced. Finally, a method of generating hairs and controlling their parameters with L-systems is proposed. The importance of these techniques is illustrated in numerous state-of-the-art plant renderings.

Acknowledgments

The rewarding task of pursuing research and writing a Masters thesis has depended on the generous support of numerous individuals and organizations, and I wish to sincerely thank everyone involved.

My supervisor, Dr. Przemyslaw Prusinkiewicz, has provided invaluable guidance and experience during my studies. His undergraduate graphics course inspired me to pursue research in the modeling and rendering of plants, and the journey has been most fulfilling. My co-supervisor, Dr. Brian Wyvill, encouraged me to undertake research as well and provided thoughtful feedback for my work. The renderings of plant models would not have been possible without the help of Dr. Henrik Wann Jensen, who supplied the Dali renderer and offered first-rate support. Gentlemen, it has been an honour to work with you!

Day to day life in the Jungle lab has been enriched by the cooperation, enthusiasm, and good humor of my fellow students. Their insights and comments regarding my work have been truly helpful, and their companionship during spare-time activities ranging from movie nights to hiking trips have rounded out the academic experience. I'd especially like to thank Adam Runions for providing high-order venation patterns that contributed greatly to the appearance of several synthetic plant images in this thesis.

My research has been generously funded by the Natural Sciences and Engineering Research Council of Canada (NSERC), the Informatics Circle of Research Excellence (iCORE), the Province of Alberta, and the University of Calgary. I wish to thank Dr. Przemyslaw Prusinkiewicz for providing further financial support.

Finally, I would like to thank my parents for their strong support, care, and understanding during my term as a Masters student. Though health has taken unfortunate turns for each of us during this period, we managed to face any challenges with optimism and anticipation for more scenic trails ahead.

To my parents, Hans and Lilo.

Table of Contents

List of Tables

List of Figures

List of Algorithms

Chapter 1

Introduction

Plant growth surrounds us. In the form of mighty trees, colorful flowers, or slender blades of grass, plants dominate many outdoor environments. Because plants contribute to the visual richness of a scene, either as foreground or background elements, it is desirable to generate realistic-looking plants for computer graphics applications.

The prairie crocus in Figure 1.1 is an example of a plant modeling and rendering challenge. Hairs along the stems, leaves, and sepals lend the crocus a soft and fuzzy appearance. Translucency in the violet sepals (commonly confused as petals [95]) permits light from the stamens to seep through the surface, generating a soft yellow glow. Subtle venation patterns are visible on the surface of the sepals. The color along the finger-like leaves changes gradually from green to a slightly-browned tip. Shadow areas below the sepals appear darkened, but do not conceal details completely. All these effects are important considerations when attempting to improve the realism of a synthetic plant model.

1.1 Problem Statement

L-systems, because of their ability to compactly describe branching structures, are commonly used for the modeling of plants. In the quest for realistic computer generated images, modeling is only one stage of the process. Equally important are rendering considerations that lend the plant model a convincing appearance. While L-systems encode geometric information in a string, they have not traditionally provided a comprehensive means of encoding rendering information. In addition, applications that deal with realistic synthesis of plants require models that can handle details textured onto or protruding from the surface, such as veins and hairs. Modeling plants from a purely geometric standpoint us-

Figure 1.1: The prairie crocus presents many modeling and rendering challenges, including hairs, translucency, veins, and gradual variations in color.

ing L-system strings is a well-studied problem. The problem of incorporating rendering information in L-systems and addressing surface details in the form of textures and hairs requires further attention.

1.2 Contributions

The overall contribution of this thesis is the introduction of a number of techniques that improve the realistic rendering of plants modeled using L-systems. A new construct, the "material module", is presented, making it possible to dynamically specify materials during L-system interpretation. Parameters passed to the material module indicate what kind of shader is to be used and what the shader's rendering parameters are. This results in the creation of a new material associated with the underlying surface generated by the L-system. Some materials require the use of a texture, necessitating the proper handling of texture coordinates in the surface. A method for fitting a texture precisely onto a

generalized cylinder is presented, taking into account the contour of the cylinder to avoid non-uniform spacing of the texture coordinates. These texture coordinates are used as the basis of procedural shaders for generating translucent edges and parallel venation patterns, whose parameters can be encoded in the L-system string via material modules. Texture mapping of more complex venation patterns with bump mapping is also examined. In order to properly shade the plant surfaces, a simple shader for leaves and petals is introduced. This shader takes into account translucency and reflective properties of plant surfaces. Finally, a method for generating hairs that protrude from the surface of the plant mesh is introduced. Numerous synthetic plants modeled with CPFG [31, 80, 78, 81] and rendered with Dali [36] are included throughout the thesis to illustrate the importance of the new techniques.

1.3 Thesis Overview

Chapter 2 contains background information about L-systems and their implementation using turtle geometry. An overview of rendering is presented in Chapter 3, both from a theoretical and an applied standpoint. The shortcomings of specifying materials in L-system implementations is discussed in Chapter 4, followed by a proposed solution involving material modules. To achieve more realistic shading of plant surfaces, effective use of skylight illumination and implementation of a leaf-and-petal shader is discussed in Chapter 5. Information about leaf structure and light interactions with plant tissues is used as a basis of the shader. In Chapter 6, texture mapping of generalized cylinders is discussed, and procedurally-based venation shaders are introduced as a means of adding surface detail to leaves and petals. The incorporation of hairs into plant models generated using L-systems is discussed in Chapter 7, along with a method for mapping hairs onto generalized cylinder surfaces and controlling hair parameters. Finally, Chapter 8 contains a discussion of results and probes future directions for research in realistic plant rendering.

Chapter 2

L-Systems

L-systems, named after their founder Aristid Lindenmayer [52], provide an elegant means of modeling the development of plants. At the heart of L-systems is a string-rewriting mechanism, which allows individual symbols in a *string* to be replaced by strings of new symbols. A *symbol* can be used to denote a cell or organ in a plant, and the replacement of the symbol by a successor sub-string may represent cell division or growth of plant structure. L-systems provide a means of characterizing the topology of a plant at every stage of its growth. Geometric aspects may be considered by interpreting L-systems using turtle geometry [74]. Programs that implement L-systems and turtle geometry can associate symbols and optional parameters with drawing commands, making it possible to visualize plant structures. This section begins by describing L-systems at the topological level. We then describe the implementation-specific details of L-systems for controlling geometry and rendering properties.

2.1 Topology

L-systems compactly describe the topology or overall structure of plants [81]. The position of symbols in an L-system string corresponds to the relative locations of plant organs. The initial string of symbols is known as the *axiom*. As plants grow, new organs emerge, resulting in more complex plant structure. At every time step, L-systems generate new sequences of symbols by applying various *productions* or *rewriting rules* to a string. The preceding string may be the axiom or a descendant string resulting from the previous application of productions. The newly generated string, in turn, is passed back to the set of productions at the next time step.

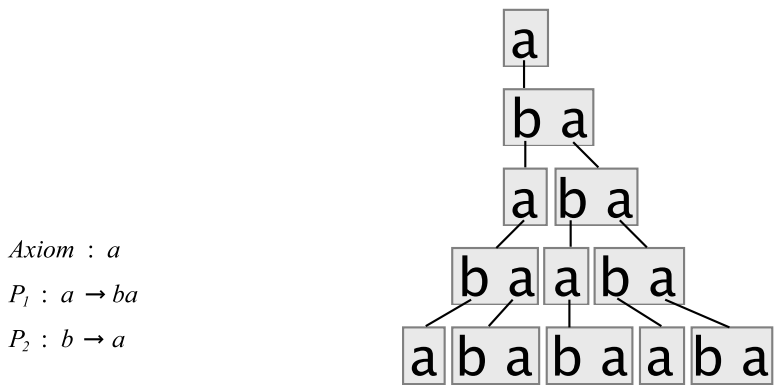

(a) (b)

Figure 2.1: Derivation of an L-system.

A production P takes a predecessor symbol *pred* and replaces it with a successor string of symbols *succ*, as follows:

$$P : \ pred \rightarrow succ$$

Figure 2.1 shows the derivation in an L-system consisting of two simple productions. The axiom consists of the single symbol a, which is matched by the predecessor of the first production, producing the successor string ba. During the next time step, we apply productions on ba in parallel. The first symbol b becomes a, while the second symbol a becomes ba, to produce the string aba. At the third time step, productions continue to be applied to each of the symbols in the new string, and the process continues for subsequent time steps. In order to terminate growth of the string, a maximum number of derivation steps is usually specified.

The application of a simple production requires only that a symbol in the incoming string match the predecessor symbol. Productions may optionally impose more rigorous conditions before they are applied. Various forms of these conditions can be seen in several types of L-systems:

- *Parametric L-systems* [31, 77] make it possible to associate symbols with one or more

parameters. A symbol together with parameters is known as a *module*. Productions may use these parameters to evaluate a boolean condition β. The predecessor will be replaced with the successor only if the boolean condition evaluates to true:

$$P: \ pred \ \{block_1\} \ \beta \ \{block_2\} \rightarrow succ$$

The optional $block_n$ statements are used to calculate variables that can be used in the condition or as new parameters for modules. The first block is executed prior to the evaluation of the condition, while the second block is executed only if the condition turns out true.

- *Context-sensitive L-systems* [52, 81] apply productions based on the context of the predecessor in relation to neighbouring symbols in the string. The predecessor must occur immediately after a matching left context lc and immediately before a matching right context rc in order for the production to proceed:

$$P: \ lc < pred > rc \rightarrow succ$$

- *Stochastic L-systems* [81] make it possible to specify the probability *prob* that a production will be applied:

$$P: \ pred \rightarrow succ \ : \ prob$$

These various types of L-systems are not mutually exclusive, and a single production may utilize a combination of boolean, context-sensitive, and stochastic conditions. For example, the following production

$$A(x) < B(y) > C(z): \ \{m = x + 1\} \ m > z \ \{n = z - 1) \rightarrow A(m)B(n) \ : \ 0.5$$

replaces module B with the module string AB, provided that B occurs between modules A and C, and variable m is greater than parameter z. Furthermore, should these conditions be

met, a stochastic evaluation will determine whether or not the production will be applied. If the production is applied, the newly computed variables m and n are used as parameters for the modules in the resulting string.

The repetitive application of productions results in an ever-changing string, representing a sequential ordering of symbols and modules. Plant structure, however, is rarely purely sequential because of branching. In order to characterize branching in a string of symbols, *bracketed notation* is utilized. Two specially defined symbols delimit a branch in a string [52]:

[Left bracket begins a branch.

] Right bracket ends a branch.

Pairs of brackets can be nested to an arbitrary degree, to represent higher-order branching structures. The entire string segment between a left and right bracket, including all nested brackets, describes a *branch*. The string segment between a left and right bracket, excluding all nested brackets and strings therein, describes the branch *axis*.

2.2 Geometry

While topological considerations help define an abstract model of a structure, the geometric treatment of L-systems makes it possible to use quantitative data for constructing and visualizing a structure. As we move from the realm of theory to geometric implementation, certain symbols in an L-system string serve as drawing commands for a LOGO-style *turtle* [1, 90, 74]. In parametric L-systems, modules include parameters that provide quantitative information for manipulating the turtle.

The turtle defines a right-handed local coordinate frame consisting of three orthogonal vectors: *heading* $\overrightarrow{H}$, *left* $\overrightarrow{L}$, and *up* $\overrightarrow{U}$ (see Figure 2.2). The turtle moves forward in discrete steps along its heading vector. By reorienting the coordinate frame at every step, the turtle

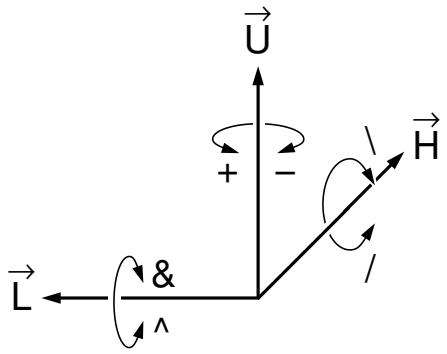

Figure 2.2: Turtle coordinate frame, displaying its three axes, as well as the modules required to rotate the turtle around them.

Module	Purpose
F(x) f(x)	move the turtle forward x units, with or without drawing a line segment
$+(x)$ $-(x)$	rotate the turtle around its heading axis by x degrees
$\&(x)$ $\hat{}(x)$	rotate the turtle around its left axis by x degrees
$/(x)$ $\backslash(x)$	rotate the turtle along its up axis by x degrees

Table 2.1: Modules for moving and reorienting a turtle.

can trace a curve through space. The software environment CPFG [31, 80, 78, 81] is able to generate strings of modules with L-systems and to graphically interpret them based on this formal notion of turtle geometry. Some basic modules for controlling the turtle are displayed in Table 2.1.

By sweeping out a contour and controlling its width, the moving turtle can produce a *generalized cylinder* [58, 82]. The turtle's path defines the *axis* of the cylinder. Closed contours are used to produce closed generalized cylinders that represent volumetric organs such as stems or branches. Other plant organs such as leaves and petals resemble thin surfaces, and have cross sections described by open contours. These organs are best represented by open generalized cylinders. Closed generalized cylinders expose only their front surface, while open generalized cylinders can expose both front and back. In addition, open generalized cylinders have edges that may represent the rim of a leaf or petal. The distinction between front, back, and, edge is important for shading surfaces (Chapter 5)

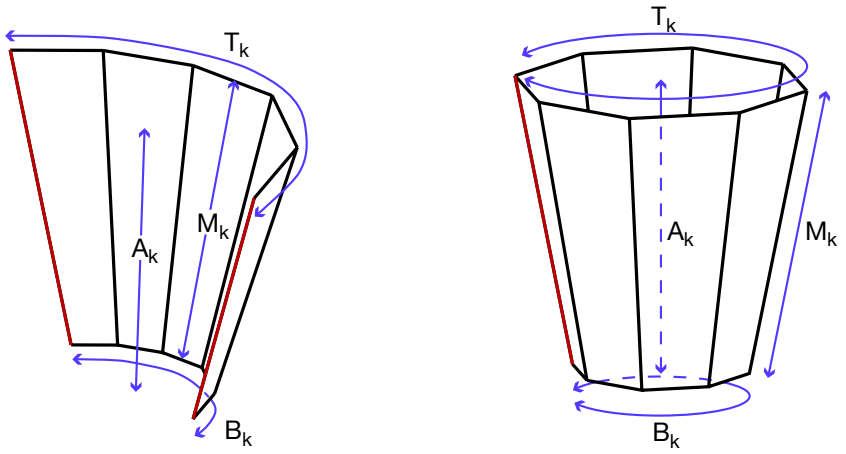

Figure 2.3: Diagram of the kth segment of (a) an open generalized cylinder and (b) a closed generalized cylinder. The outer edges of the open segment and seam of the closed segment are shown in red. T_k and B_k are the length (or circumference) of the top and bottom rims of the segment, respectively. The length of the axis is denoted A_k. The *mid-arc* of a cylinder is a line segment joining the midpoint of the top rim and bottom rim. The length of the mid-arc is denoted M_k.

---

and placing hairs (Chapter 7).

Generalized cylinders are polygonized into sequences of connected *segments*, where each segment corresponds to a step taken by the turtle [58]. These segments consist in turn of a strip of quadrilateral *faces* that approximate the cylinder shape defined by the contour. In the actual implementation, each quadrilateral face may consist of two joined triangles, but for the purpose of discussion, we will assume that each face is a quadrilateral. A quadrilateral strip for an open cylinder segment has a top and bottom *rim* running between the strip's two outer edges. On a closed cylinder segment, these edges are joined along a seam. Cylinder segments with open and closed contours are shown in Figure 2.3, along with several measurements.

CPFG provides several modules to manipulate generalized cylinders [58]. The module @Gs begins a generalized cylinder, @Gc instructs the turtle to sweep out a cylinder segment during its next step, and @Ge ends the cylinder. The contour tracing out the generalized cylinder can be scaled by a factor of s using the module !(s).

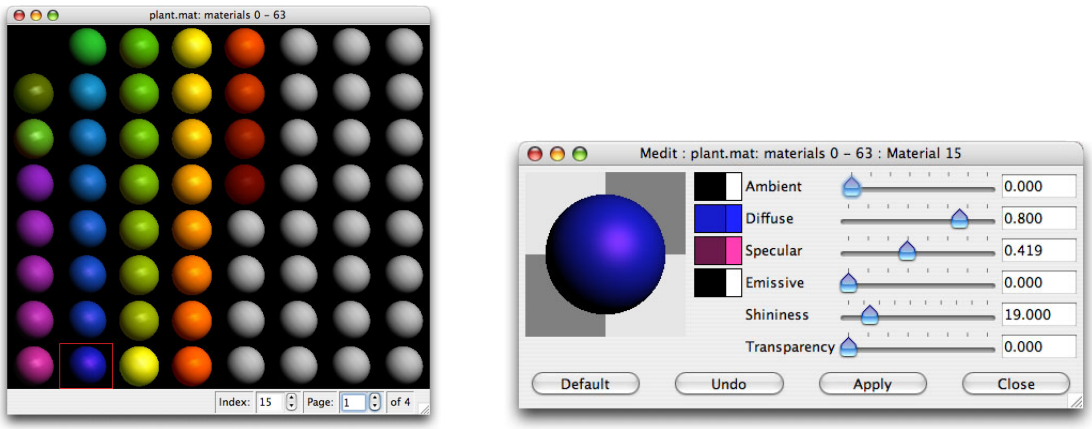

Figure 2.4: The material table and material properties as seen in the medit editor [19].

Certain lobed structures cannot be modeled by generalized cylinders, and are more easily modeled using Bezier patches. The module ˜(p, s) places a Bezier patch p, and scales it by factor s.

2.3 Rendering

Using the modules discussed thus far, it is possible to construct a geometric mesh of a plant or its constituent organs. For realistic visualization, we must be able to shade the mesh. This can be achieved by introducing several modules for rendering purposes.

Surface materials can be specified with the module ;(x). The parameter x indexes a table with material presets (Figure 2.4). The material presets used by CPFG are all based on the Phong model [9]. For each material, ambient, diffuse, and specular colors can be defined, along with values for shininess and transparency.

Plant surfaces rarely have one solid color. Normally, there are subtle color gradations along a stem or leaf. Gradations can be simulated by defining a range of gradually changing materials in the color table, and changing the color index for every successive generalized cylinder along the plant organ. However, even gradations cannot capture more complex surface features, such as venation patterns or bark. For these purposes, texture mapping

is desirable, and CPFG can index a texture x using the module $@Tx(x)$ [58, 59]. CPFG will either overlay or blend the texture with the current material. The use of texture mapping to add more detail to plants is discussed further in Chapter 6.

2.4 The Turtle Dispatcher

In order to visualize the results of an L-system, the drawing commands issued by symbols or modules need to be sent to a rendering system. The actions defined by these drawing commands are sufficiently high-level that a variety of rendering systems can be supported. For every renderer, all that is required is a *rendering interpreter* that translates turtle commands into function calls or statements supported by the renderer. CPFG provides a *turtle dispatcher* interface, consisting of virtual function headers for every drawing command. A rendering interpreter must implement each of these functions. When CPFG interprets an L-system and encounters a particular drawing command, it calls the corresponding function for the currently active interpreter. Conceptually, a turtle command has been issued, and the rendering interpreter intercepts the command. For example, if CPFG is currently rendering to OpenGL, the $;(x)$ module will trigger a "change material" command, which gets dispatched to the material function in CPFG's OpenGL interpreter in order to issue a glMaterial() call. When real-time rendering systems such as OpenGL are employed, the drawing commands are immediately carried out, producing graphical results in a framebuffer. Offline rendering systems, such as Dali and Renderman, require the rendering commands to be written to a file which is processed at a later time when the renderer is invoked.

Chapter 3

Rendering Fundamentals

In order to synthesize realistic images in computer graphics, it is essential to simulate the proper passage of light through a scene and to model interactions with materials when light strikes a surface. After a discussion of terminology related to light propagation, we will examine light-material interactions and examine the progression of rendering systems toward global illumination solutions.

3.1 Radiometry

The body of work concerned with the measurement of radiant energy transfer is known as radiometry. While the field of radiometry covers the entire spectrum of radiant energy from radio waves to gamma rays, in image synthesis we are concerned in particular with visible light. This section presents some of the important terminology introduced by radiometry.

Light is often described in terms of *wave-particle duality* [3]. Certain characteristics of light, such as interference, diffraction, and polarization, can only be described by wave phenomena. On the other hand, a particle analogy is required to explain the photoelectric effect, whereby electrons are ejected from a surface upon the application of light. This dual nature makes it necessary to describe light in terms of both waves and particles.

Light travels as packets of energy called *photons*, which have a particular wavelength λ. The energy e_λ of a photon can be computed through the use of Planck's constant h and the speed of light c:

$$e_\lambda = \frac{hc}{\lambda} \tag{3.1}$$

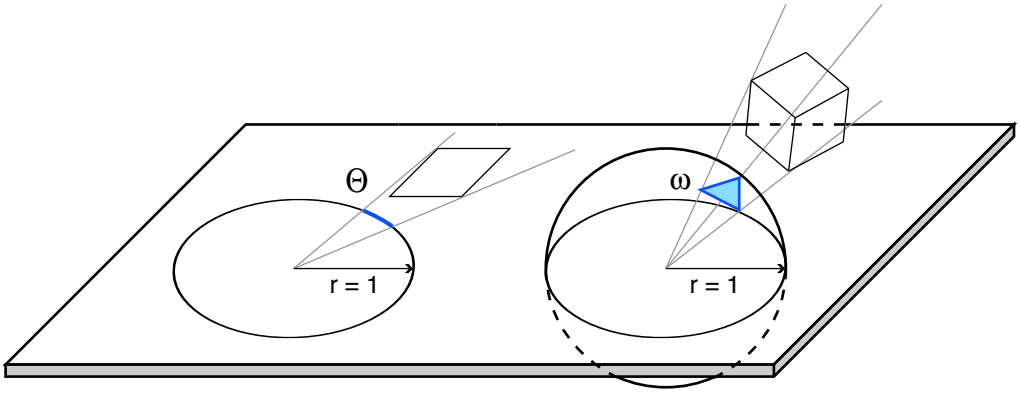

Figure 3.1: Definition of angle Θ and solid angle ω. Angle is the arc length of an object's projection onto a unit circle. Solid angle is the surface area of an object's projection onto a unit sphere.

Given a light beam with n_λ photons of wavelength λ, the *spectral radiant energy* Q_λ is:

$$Q_\lambda = n_\lambda e_\lambda \tag{3.2}$$

Visible light is usually composed of photons of many different wavelengths. By integrating over all wavelengths, we can compute *radiant energy* Q:

$$Q = \int_0^\infty Q_\lambda d\lambda \tag{3.3}$$

In order to emphasize the flow of radiant energy over time, we can define *radiant flux* Φ:

$$\Phi = \frac{dQ}{dt} \tag{3.4}$$

Radiant energy leaving a surface, either through emission, reflection, or transmission, may do so at different rates for different points on the surface and in various directions in the hemisphere above the surface. It is therefore important to consider differences in radiant flux from point x in a given direction $\vec{\omega}$.

If the hemisphere is centered at x and has a radius of one, then the flux traveling in direction $\vec{\omega}$ passes through a small region of the hemisphere's surface. The surface area of this region is the solid angle. More formally, the *solid angle* subtended by an object

from a point x is defined to be the surface area of the projection of the object onto a unit sphere centered at x. A solid angle is a generalization of the concept of an angle in two dimensions to three dimensions (Figure 3.1). Angles are measured in radians, and solid angles in *steradians* (sr). In the same way that the angle subtended by an enclosing circle is 2π rad (the circumference of a circle), the solid angle subtended by an enclosing sphere is 4π sr (the surface area of a sphere).

Radiance L is the radiant flux per unit area perpendicular to the direction of travel, per unit solid angle:

$$L(x, \vec{\omega}) = \frac{d^2\Phi}{\cos\theta \, dA \, d\vec{\omega}} \tag{3.5}$$

Conceptually, radiance is a measure of the number of photons arriving at or leaving from a small area in a particular direction (Figure 3.2). Spectral radiance L_λ is a measure of radiance for photons of a certain wavelength λ (i.e. light of a particular color).

If we integrate radiance over all directions, we are able to compute *radiosity* B, the flux leaving a point x, and *irradiance* E, the flux arriving at a point x:

$$B(x) = E(x) = \frac{d\Phi}{dA} \tag{3.6}$$

Radiance, radiosity, and irradiance are important entities in computer graphics, as they provide a means of expressing light transfer between light sources and objects. We shall now consider what happens when light actually hits an object.

3.2 Light-Material Interactions

Light traveling toward an object consists of photons of particular wavelengths. The coloration of this light, as perceived by a viewer, depends on the photons' wavelengths, while the intensity of the light depends on the number of photons. When light strikes the object's surface, the photons interact with the material in different ways.

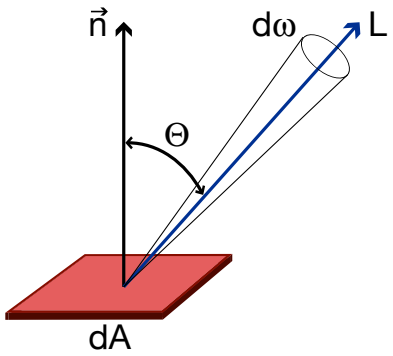

Figure 3.2: Definition of radiance L. Radiance is radiant flux per unit projected area dA per unit solid angle $d\vec{\omega}$.

A material can be thought of as a volumetric collection of small particles suspended in a medium [71] (Figure 3.3). If these particles are packed tightly together, an incoming photon is unable to penetrate the material and will reflect directly from the surface. If the particles are loosely packed, the photon may pass partially through the medium before colliding with a particle. During a photon-particle collision, the photon may be selectively absorbed depending on its wavelength [3]. The net effect is that more photons of certain wavelengths are absorbed than photons of other wavelengths, and the color of the light changes. A photon may undergo several successive collisions with particles before emerging from a different point on the surface; this phenomenon is called *subsurface scattering*. Alternatively, light may completely miss particles, retaining its original color but emerging with a reduced intensity, due to photon absorption in the medium.

Interactions between photons and materials result in reflected or transmitted light having a different radiance than incoming light. Calculating this change in radiance is an important step for determining the appearance of a surface. In general, the outgoing radiance L_o in direction $\vec{\omega}$ from point x on a surface can be computed as follows:

$$L_o(x, \vec{\omega}) = L_e(x, \vec{\omega}) + L_r(x, \vec{\omega}) + L_t(x, \vec{\omega}) \tag{3.7}$$

where L_e is emitted radiance, L_r is reflected radiance, and L_t is transmitted radiance.

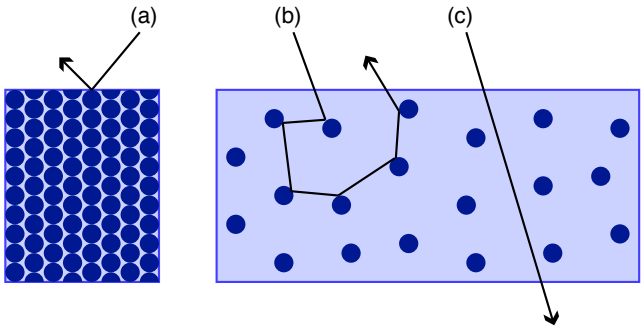

Figure 3.3: Light-material interactions shown in cross-section. Photons striking the material may follow one of several paths. In (a), a photon is reflected at the surface after a single collision with a particle. In (b), a photon penetrates the material and subsurface scattering takes place due to collisions with multiple particles. In (c), no particle collisions take place.

Emitted radiance need only be considered if the material emits energy, as in the case of a heated element or phosphorous compound. For materials that do not emit energy, only the reflected and transmitted radiance terms are of interest.

The reflected radiance depends on all the incoming radiance L_i arriving from various directions $\vec{\omega}'$ within the hemisphere Ω above the surface:

$$L_r(x, \vec{\omega}) = \int_{\Omega} f_r(x, \vec{\omega}', \vec{\omega}) L_i(x, \vec{\omega}')(\vec{\omega}' \cdot \vec{n}) d\vec{\omega}' \tag{3.8}$$

The term $(\vec{\omega}' \cdot \vec{n})$ is required according to *Lambert's Law*, which states that a light source directly above a surface delivers the most radiance, while radiance gradually decreases as a light source sets toward the surface's horizon. The incoming radiance must be scaled by the factor f_r to account for energy absorbed by the surface. This factor is known as the *BRDF* (*Bidirectional Reflectance Distribution Function*) [66], if we assume that light arrives and leaves at the same point on a surface.

Formally, a BRDF is the ratio of reflected radiance to irradiance:

$$f_r(x, \vec{\omega}', \vec{\omega}) = \frac{dL_r(x, \vec{\omega})}{dE_i(x, \vec{\omega}')} \tag{3.9}$$

and has units of sr^{-1}. In this way, a BRDF can be considered to be a density function, describing the attenuation of radiance per unit steradians. The function can be visualized

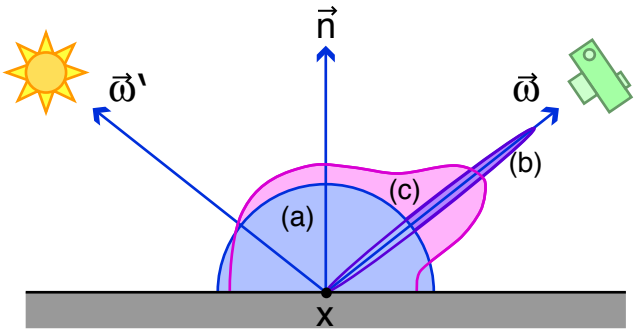

Figure 3.4: A BRDF attenuates the radiance arriving from direction $\vec{\omega}'$ and leaving in direction $\vec{\omega}$. (a) A BRDF for ideal diffuse reflection scatters light equally in all directions. (b) A BRDF for ideal specular reflection scatters light in the mirror direction only. (c) BRDFs in nature are often a mixture of the first two cases.

---

for a hemispherical region above a point (Figure 3.4). In ideal diffuse reflection, light is reflected equally in all directions, producing a BRDF with a smooth dome of constant radius. In ideal specular reflection, light is reflected in a sharp peak. More commonly, surfaces exhibit a mix of ideal diffuse and specular reflection, producing a BRDF with a lobe protruding in the general direction of specular reflection. Small variations in the surface of a BRDF represent non-uniform scattering of light due to surface roughness.

The BRDF can be replaced by a *BSSRDF* (*Bidirectional Scattering Surface Reflectance Distribution Function*) $f_r(x', x, \vec{\omega}', \vec{\omega})$, if we take into account subsurface scattering and assume that light can arrive at point x' and leave at a separate point x. For transmissive materials, radiance may similarly be scaled by a *BTDF* $f_t(x, \vec{\omega}', \vec{\omega})$ or *BSSTDF* $f_t(x', x, \vec{\omega}', \vec{\omega})$, where T stands for transmittance and light is assumed to arrive and leave on opposite sides of a surface. A BRDF and BRTF collectively define a *BDF* (*Bidirectional Distribution Function*), and a BSSRDF and BSSTDF collectively define a *BSSDF* (*Bidirectional Scattering Surface Distribution Function*) [27]. The BDF (or BSSDF) accounts for the visual properties of materials.

Two methods are commonly used to determine a BDF. First, BDFs may be computed algorithmically. Early computed BDFs were phenomenological (e.g. Phong reflection model

Symbol	Terminology	Representation/Unit
x	Position	coordinates
x'	Position of incoming radiance	coordinates
$\vec{n}$	Surface normal	normalized vector
$\vec{\omega}$	Direction of outgoing radiance	normalized vector
$\vec{\omega}'$	Direction toward source of incoming radiance	normalized vector
$d\vec{\omega}$	Differential solid angle	sr
λ	Wavelength	nm
Q	Radiant energy	J
Q_λ	Spectral radiant energy	$\frac{J}{nm}$
Φ	Radiant flux	W
B	Radiosity (outgoing)	$\frac{W}{m^2}$
E	Irradiance (incoming)	$\frac{W}{m^2}$
L	Radiance	$\frac{W}{m^2 sr}$
f_r	BDF	$\frac{1}{sr}$
f_t	BSSDF	$\frac{1}{sr}$

Table 3.1: A summary of symbols and terminology introduced in this chapter.

[72]) or physically-based (e.g. Torrance-Sparrow microfacet model [92]), and considered surface reflection only. BSSDFs that compute the attenuation of radiance during single-scattering [32, 47] and multiple-scattering [38] increase cost but improve appearance of surface. Alternatively, BDFs can be measured directly from acquired data of real materials in nature. Light and camera arrays together with turntables for rotating the material samples can be used to capture reflected radiance for various viewing and illumination angles [97, 53, 56]. Once a library of BDFs for different materials has been obtained, linear combinations of BDFs may be used to simulate light interactions in new materials [57].

The terms and symbols reviewed in this chapter have been summarized in Table 3.1.

3.3 Rendering

The task of a renderer is to perform a simulation of all light exchange in a scene, so that precise radiance values are determined at any point on a surface. During the generation of an image, the incoming radiance from a surface point is used to determine a pixel's

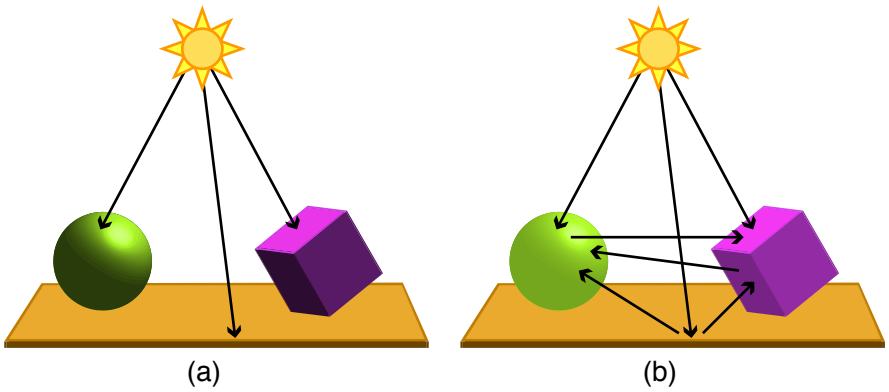

Figure 3.5: In direct illumination (a), surfaces are illuminated only by light arriving directly from light sources. Indirect illumination (b) takes into account reflected light from surrounding surfaces.

---

intensity. In radiometry applications, radiance is a spectral measurement for light over a continuous spectrum of wavelengths. In rendering applications, spectral measurements are often represented as vector-valued quantities consisting of three "wavelengths": red, green, and blue. The advantage of this approach is that radiance values can be directly represented as colors in RGB space. In the remainder of this thesis, RGB values for pixels on an image are assumed to represent incoming radiance measurements.

Modern rendering systems typically split up the rendering process into two components, the light transport algorithm and the shading algorithms [12]. In early renderers, the light transport algorithm propagates radiant energy only from the light sources to surfaces in a scene (*direct illumination*). This fails to capture interreflections between objects, resulting in images with unusually dark shadows. Light transport in more sophisticated renderers supports *global illumination*, whereby radiant energy is also propagated between surfaces (*indirect illumination*) (Figure 3.5). When light rays hit a surface, the shading algorithm takes effect, using the BDF or BSSDF to determine how much of the incoming radiance will be reflected and transmitted back into the environment.

Traditional ray tracing [99, 44] gathers radiance from reflection and refraction rays that travel around a scene, obeying physical principles such as perfect mirror reflections

and Snell's Law. Every time a ray hits an object, shadow rays are spawned to sample light sources directly and check for impeding objects. The algorithm is recursive, allowing rays to follow reflected and refracted paths to an arbitrary depth. Objects, reflections, and shadows in the resulting images appear very crisp, to the extent that they no longer look natural. By splitting a ray into multiple rays and using stochastic sampling to find the average radiance, distribution ray tracing [14, 13] made it possible to render fuzzy phenomena such as gloss, translucency, depth of field, and motion blur. Multiple shadow rays could be used to sample area light sources, producing soft shadows.

Early ray tracing techniques did not simulate illumination due to diffuse reflections from surroundings. The problem was simultaneously addressed in two publications [29, 67] through the use of finite elements. The surfaces in a scene are subdivided into tiles, and exchanged radiant energy between tiles is computed by solving a system of linear equations. This technique is the foundation of radiosity methods, which make it possible to compute view independent global illumination solutions. However, radiosity methods are costly for complex models with many tiles and non-diffuse surfaces. Taking inspiration from distribution ray tracing, Kajiya [40] proposed the use of stochastic sampling to gather reflected radiance from surrounding surfaces in ray tracing methods. Because of the recursive nature of ray tracing, the number of sampling rays increases exponentially as the depth of reflections increases. To prevent this situation, Kajiya presented a solution called path tracing (Figure 3.6). Whenever a ray hits a surface, only a single stochastic ray is chosen to estimate the indirect illumination.

Pixels in an image produced by path tracing must be supersampled to ensure that sufficient stochastic paths have been followed for a reasonable estimation of reflected radiance. If too few paths are followed, variances in the estimates result in noisy images. For scenes with complex illumination, pixels may need to be sampled with hundreds or thousands of paths to produce acceptable images. Photon mapping [35] considerably improves perfor-

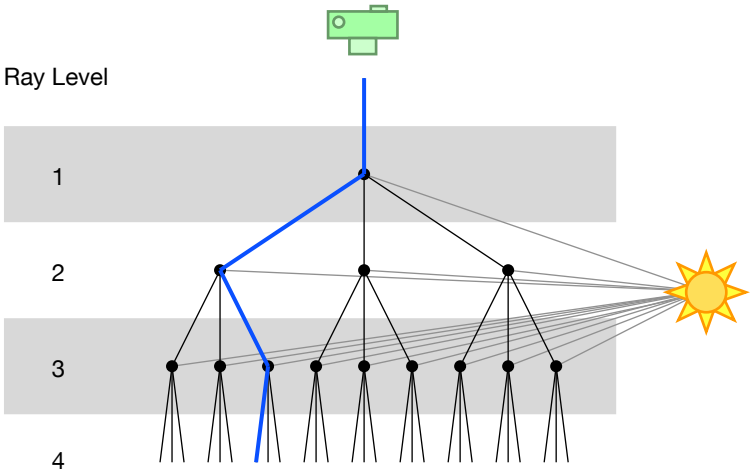

Figure 3.6: In order to sample surroundings for indirect illumination during ray tracing, sampling rays can be sent into the environment at every recursive step. In this example, three rays are spawned at every step, along with an additional shadow ray that samples a direct light source. This leads to an exponential growth in the number of sampling rays. Path tracing improves performance considerably by tracing only a single path (shown in blue) in the ray tree.

---

mance by using a caching strategy prior to path tracing. Photons associated with radiance values are sent out from light sources, traced through the scene, and stored in the photon map whenever they are absorbed by a surface. During path tracing, a ray intersecting a surface can obtain a radiance value from the photon map rather than having to spawn an additional sampling ray. The renderings in this thesis employ path tracing, and in some cases photon mapping, to achieve global illumination.

Chapter 4

Dynamic Specification of Materials

This chapter discusses two concepts that lie at the heart of rendering techniques: shaders and materials. The current deficiencies in support for shaders and materials in the realm of L-systems are outlined and discussed. The dynamic specification of materials and their parameters in the context of L-systems is then proposed.

4.1 Shaders

The process of rendering involves shading surfaces so that they assume a desired appearance. Just as there is literally an endless variation of possible surface appearances, shading algorithms are limited only by the imagination of the shader writer. Whether the goal is to create a realistic backlit arbour of leaves or an artistic charcoal rendition of a flower, the act of shading a surface requires computing intensity values for pixels in the final image.

A *shader* is a subroutine that defines a BDF or BSSDF so that the outgoing radiance from a point on a surface can be computed based on incoming radiance. Early renderers [100] compiled shader subroutines directly into the codebase, making it difficult to extend a renderer with new shaders. Cook [12] recognized shaders as independent, modular entities that could be separated from the light transport algorithm of the renderer. Many rendering programs subsequently provided support for their own shading languages [94, 68, 55, 87] and allowed shaders to be compiled and loaded as independent modules.

Each shader requires a set of *appearance parameters* [12] used by the BDF calculation. Appearance parameters can by *varying* or *uniform* [33]. Varying parameters may change for every point that requires shading. Examples of varying parameters include the shading normal and *uv*-coordinates. Shaders typically obtain the varying parameters directly from

the renderer. Uniform appearance parameters remain constant wherever a shader is applied. They are typically supplied by the user, and specify properties such as diffuse color, specular color, and translucency. A uniform appearance parameter does not imply a uniform surface appearance. For example, the endpoint colors of a gradient may be uniform appearance parameters, but the shader can interpolate between these colors to generate a surface that appears anything but uniform.

In this thesis, we call the list of uniform appearance parameters along with their data types a *shader description*. The shader description separates the list of parameters required by the shader from the underlying implementation.

This high-level treatment of shaders is useful, since shaders are typically not compatible between rendering systems. One notable exception is the family of rendering systems based on the Renderman interface [94], making it possible to write a single shader that works under multiple systems. However, many other rendering systems either provide a built-in set of shaders or provide their own custom shading language or API for building shaders. While these shaders cannot be swapped between systems because of varying implementations, their shader descriptions are often very similar. For example, Phong shaders that require a diffuse color and a specular color, along with a specular highlight coefficient, can have an identical shader description, even though the shaders may be locked into their rendering system at an implementation level.

When all of the uniform parameters in a shader description have been specified, they are said to be *bound* [33], and a shader instance, or *material*, has been created (see Figure 4.1). In this way, shaders and materials are analogous to the concept of classes and objects in object-oriented programming languages. Shaders provide the engine for generating a class of surface appearances, and they have a clearly defined shader description (similar to a class interface). Materials, similarly to objects, add the specific parameters required to produce a particular surface. In the same way that a class interface is designed to hide

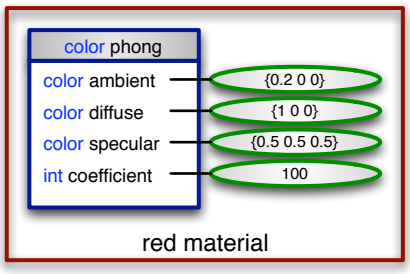

Figure 4.1: A material is formed when a shader's appearance parameters are bound to specific values. This diagram depicts a reflective, red material based on a Phong shader in the Dali renderer. The blue box is the shader description, which lists the appearance parameters and indicates that the Phong shader returns a color.

---

the complexity of a class' implementation from the user, shader descriptions indicate what values must be supplied, without requiring detailed knowledge of how these values are used in the shader's rendering calculations.

4.2 Rendering Limitations in L-systems

In order to visualize an L-system model, the modules in an L-system string must be graphically interpreted. Rendering may take place in real-time, if technologies such as OpenGL [87] are used, or it may be deferred for high-quality, offline rendering. If a real-time system is used, L-system modules and their parameters must be immediately translated into rendering instructions and passed via memory to the renderer. For offline rendering systems, these instructions are usually written to a file whose format conforms to the renderer's specifications. The file is then processed by the renderer at a later time.

What is the nature of the rendering instructions? Besides setting up camera and lighting information, they describe two key pieces of information about the model. First, they specify the geometry of the model, by defining various transformations and describing surfaces in the form of polygonal meshes or parametric surfaces. Second, the instructions specify the materials that are used to shade various parts of the model.

L-systems have traditionally been used as a modeling tool [75, 79, 58, 82, 43], and conse-

Figure 4.2: The stem of the snowlily varies in color along its length.

quently the majority of modules are associated with instructions related to the construction of the plant's geometry. However, from the perspective of realistic plant rendering, believably shaded surfaces are just as important as well-defined geometry. In nature, plants exhibit a diverse range of possible materials, from matte woody surfaces to translucent leafy tissues. Material properties may change gradually along a single organ (Figure 4.2). Prior to this research, no robust modules existed for setting the appearance of surfaces. As discussed in Section 2.3, L-systems as implemented in CPFG are able to index Phong materials in a predefined table and load textures from files. The materials generated by such implementations are static (they are unable to make use of values computed during L-system derivation) and do not take advantage of the wide range of shaders and appearance parameters that may be supported by the rendering system. In the case of offline renderers, the rendering files generated during L-system interpretation usually need to be edited in a post-processing stage (manually or with the help of an automated tool) to define more advanced materials. For real-time renderers, no L-system modules exist to directly invoke

a desired shader with specific parameters. In short, a new mechanism is required to allow L-system models to provide detailed information about materials. Together, geometry and material parameters serve to comprehensively describe the visual nature of a plant within an L-system.

4.3 Requirements

Several requirements should be met when specifying new materials from an L-system.

- **Support for arbitrary shaders.** It should be possible to specify any shader supported by a rendering system. Shader descriptions provide a high-level interface between the L-system and the shaders of the underlying rendering system.

- **Support for multiple appearance parameters.** Because shaders may require anywhere from zero to several dozen appearance parameters, it should be possible to specify an arbitrary number of parameters for a new material.

- **Dynamic declarations.** It should be possible to generate new materials on the fly, using parameters that are calculated during the derivation of the L-system. A predefined table of static materials, such as the material table used by CPFG, is not sufficient by itself, although it could be used in conjunction with dynamic material declarations.

- **Compatibility with multiple rendering systems.** Because a single L-system can be used to generate plant models for several rendering systems, it must be possible to indicate which systems the materials are targeted toward.

The overall goal is to be able to specify any material at any point during L-system interpretation, for any supported rendering system. The solution found during the course of this research is presented in the remaining sections.

4.4 Material Modules

In order to specify a new material dynamically, it must be specified within the L-system. Variables computed during L-system derivation can then be utilized as parameters for the material. We define a *material module* to provide information about the new material. Two important parameters are s, the name of the shader, and $p = \{p_1, p_2, \ldots, p_n\}$, the set of appearance parameters:

$$@Mt(s, p)$$

The number and types of parameters that a particular shader can accept is provided by a shader description. A shader file containing a list of shader descriptions is parsed prior to L-system interpretation. Each shader description specifies the name of the shader, followed by a list of uniform appearance parameter names and their data types. For this research, the following data types have been used: *int*, *float*, *string*, *color*, *vector*, and *shader*[1]. The first three data types reflect their counterparts in programming languages such as C++ and Java. Color and vector are three-element arrays of floats, which can be used for RGB values or normals. The shader data type references shaders, and is useful for shade tree constructs (see Section 4.6). Each appearance parameter can optionally be given a default value, to be utilized if no corresponding parameter is specified in the L-system material module.

Because an L-system can generate rendering instructions for multiple rendering systems, shader descriptions in the shader file must be associated with specific renderers. During graphical interpretation of the L-system string, only those shader descriptions associated with the target rendering system (i.e. the rendering system being used to graphically view the L-system model) are utilized. In the CPFG shader file, a list of renderers is prepended to each shader description (Figure 4.3). A shader description without a renderer list is

[1]Parameter values for L-system modules in CPFG are not typed. These values need to be cast to the appropriate data types required by the appearance parameters.

```
DALI lambert {
    color diffuse;
};

RIB matte {
    float Ka = 0.2;
    float Kd = 0.8;
    color 'color' = 0.6 0.4 0;
};

RAYSHADE DALI phong {
    color ambient = 0.2 0 0;
    color diffuse = 1 0 0;
    color specular = 0.5 0.5 0.5;
};

OPENGL GL {
    color ambient;
    color diffuse;
    color specular;
    int coefficient;
};
```

Figure 4.3: Sample shader descriptions in a CPFG shader file. Keywords are shown in blue. Each shader description is associated with one or more compatible renderers. Of the two Lambertian shaders, lambert will only be used by Dali, and matte will only be used by Renderman. Phong is supported by Rayshade and Dali. The GL shader description is targeted specifically for OpenGL. The appearance parameters for matte and phong are associated with default values. Shader or parameter names that conflict with keywords must be placed in quotes.

automatically associated with all renderers. When a material module is encountered in the L-system, rendering instructions for the material are generated only if the shader is supported by the target rendering system. If the shader is supported, rendering instructions for the new material are generated; otherwise, the material module is skipped.

Different renderers usually support shaders that perform identical or similar appearance calculations. Sometimes the shader descriptions are identical. For example, Dali and Rayshade [48] support Phong shaders with three appearance parameters specifying a color: *ambient*, *diffuse*, and *specular*. The shader file in Figure 4.3 illustrates how a single Phong shader description can be used for both renderers. More often, shader descriptions differ slightly, and two separate entries are required. For example, Dali and Renderman both support Lambertian shaders. In Renderman, the shader is called *matte*, and requires three appearance parameters: K_a (ambient reflectance term), K_d (diffuse reflectance term), and

Token	Value Referenced
%a	ambient color
%d	diffuse color
%s	specular color
%h	shininess parameter

Table 4.2: Tokens in a material module parameter list reference various properties in the currently selected material of the material table.

---

color. In Dali, the shader is called *lambert*, and requires only a *color* parameter.

When utilizing a material module within the L-system, the name of the desired shader is passed as the first parameter. Subsequent parameters are bound to the appearance parameters in the order they are listed in the shader specification. The parameters may take one of several forms:

- constants that are hardcoded directly into the parameter list. For example, in CPFG, the module @Mt("*lambert*", $0, 1, 0$) will produce green.

- variables that have been calculated within the code block of an L-system production. For example, in CPFG, the module @Mt("*lambert*", $0, g, 0$) will produce whatever shade of green is specified by the variable g.

- *tokens* that reference parameters from the currently selected material in the material table. Tokens available for CPFG have been listed in Table 4.2. Tokens provide support for referencing materials stored in material tables. For example, @Mt("*lambert*", "*%d*") will utilize the diffuse color of the current material.

- no parameters. If no parameter is specified, the default value in the shader file will be used. If no default value exists, the appearance parameter will not be included in the rendering instructions generated by the L-system. In CPFG, parameter lists in modules do not support empty spaces, so as soon as a parameter is left out, all

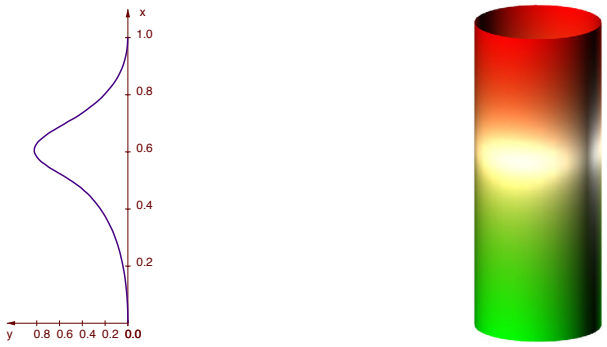

(a) (b)

Figure 4.4: An OpenGL snapshot (b) of the cylinder produced by the L-system in Algorithm 1, making use of material modules to change material properties. The function (a) was used to compute the intensity of the specular component along the length of the cylinder.

---

subsequent parameters must also be left out. For example, using the *matte* shader in Figure 4.3, it is possible to write @Mt("*matte*", 1, 0.5) to use the default parameter for color, but attempting to use the default parameter for ambient reflectance as well, by writing @Mt("*matte*", ,0.5), would produce an error.

4.5 Example: Color Gradient on a Cylinder

To demonstrate the use of material modules, we will generate the Phong-shaded cylinder shown in Figure 4.4. The cylinder gradually changes color from green to red, and has a specular highlight just past its midsection. The L-system in Algorithm 1 produces the cylinder. The first two lines set the cylinder length and the turtle's step size. The axiom on line 3 loads a static material from the table, adjusts the cylinder width, and begins the cylinder with @Gs. The production B repeatedly advances the turtle and draws a generalized cylinder segment @Gc (line 13) as long as the current position is less than the total axis length (line 4). For every step, we calculate the relative distance traveled by the turtle (line 6). In lines 7 and 8, values for red and green are set proportionally and inversely proportionally to the turtle's relative distance along the cylinder axis. A value for specular color is computed from a function in line 9. The material module in line 11

Algorithm 1 This L-system draws a generalized cylinder with changing Phong parameters for every turtle step.

1. #define l 100 /* length of axis */
2. #define Δs 1 /* turtle step */

3. Axiom: ;(1) !(40) @Gs B(0)

4. B(s): $s \leq l$
5. {
6. $relativeDistance = s/l$;
7. $r = relativeDistance$;
8. $g = 1 - relativeDistance$;
9. $s = \text{func}(1, relativeDistance)$;
10. } $\longrightarrow$
11. @Mt("GL", "$\%a$", $r, g, 0,\ s, s, s$, "$\%h$")
12. @Mt("$phong$", "$\%a$", $r, g, 0,\ s, s, s$)
13. f(Δs) @Gc B($s + \Delta s$)

14. B(s): $s \geq l \longrightarrow$ @Ge

specifies the GL shader declared in the shader file in Figure 4.3. The ambient and specular coefficient properties are specified using tokens, which reference the material loaded in the axiom. The diffuse color and specular colors are dynamically specified using the variables from lines 7 - 9. According to the shader file, the material based on the GL shader will only be generated if OpenGL is used, so another material module has been added on line 12. This module references the Phong shader description for Dali and Rayshade, so the cylinder's materials will also be generated if the L-system is graphically interpreted for either of these offline renderers.

4.6 Shade Trees

While simple shaders such as *phong* and *matte* require only several appearance parameters, complex shaders may easily require several dozen parameters that are passed through a complex rendering calculation. In order to increase the maintainability of a complex shader, it can be decomposed into smaller modular units or *sub-shaders* that perform nested operations. Sub-shaders operate conceptually like shaders, in that they generate a value based on input from appearance parameters. In this thesis, a sub-shader whose appearance parameters are bound to values is termed a *sub-material*.

Sub-shaders constituting a shader can be arranged as a *shade tree* [12]. Nodes in the tree represent sub-shaders. Each sub-shader returns a value that can be bound to an appearance parameter in the parent node. The root node must produce a radiance value in order to generate a pixel in the final image. Leaves of the tree represent parameter values. A node together with its leaves represents a sub-material.

Appearance parameters can now be obtained via explicit values, or from the value returned by a sub-shader. The appearance parameters of some types of shaders require not just a value, but a reference to the sub-shader itself. These appearance parameters are associated with the *shader* data type. Two example shaders with shader parameters (see Figure 4.5) are:

- *blend shaders*: A blend shader blends together the results of two shaders, based on the value of a weight parameter.

- *conglomerate shaders*: A conglomerate shader is a collection of several different types of shaders that function in parallel. Many rendering systems permit the use of a surface shader, volume shader, displacement shader, and shadow shader for a single material.

A shade tree is specified in an L-system using preorder traversal. Each node is declared as

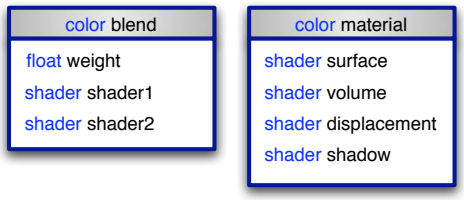

Figure 4.5: Examples of shaders with *shader* datatypes for appearance parameters.

---

a module, while leaves and links to children nodes define the module's parameters. The material declaration begins with the material module that represents the root node. For a shade tree consisting of a single node, the material description at this point would be complete. For a shade tree with more than one node, new notation is required to reference the children nodes. To indicate that a parameter will obtain its value from a sub-shader, we use a sub-material token $\%m$ in lieu of a parameter value. Subsequent nodes in the tree are specified using a sub-material module:

$$@Ms(s, p)$$

Syntactically, a sub-material module is identical to a material module. The only difference lies in function: whereas a material module returns a radiance value for shading a pixel in the image, a sub-material module satisfies a sub-material token in the parent node's parameter list by either returning a value or, for a shader data type, a reference to the sub-shader. One sub-material module is required for every sub-material token.

Figure 4.7 displays a lupine whose materials are defined using shade trees. The shade tree for leaves is illustrated in Figure 4.6. The "material" conglomerate shader describes the leaf surface based on a surface shader to generate coloration and a shadow shader to scale the intensity of light passing through surfaces (see Section 5.3.1 for further discussion on shadows). The surface shader property is bound to a bumpmap sub-shader, which combines a Phong sub-shader with the perturbations of the normals produced by a texture bumpmap sub-shader.

A portion of the leaf production for the lupine L-system is shown in Algorithm 2. The

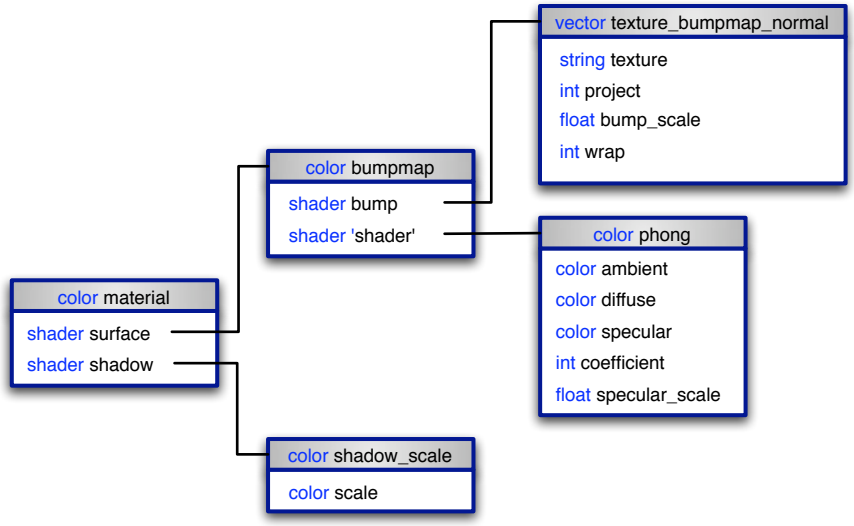

Figure 4.6: A simple shade tree used to render lupine leaves in Dali.

---

shade tree for leaf materials is shown in lines 10 to 14. The sub-material modules have been indented to reflect the traversal of the shade tree.

Materials parameters are dynamically specified using positional information. Organ features frequently vary as a function of position on a plant. While positional information was previously used to adjust geometric features [82], here it is used to influence rendering parameters. The lupine's stem and leaf color have been set as a function of position along the plant's axis, with lower leaves appearing yellowish. As we move upward along the plant, we adjust the leaf coloration to increasingly deeper shades of green. We give young leaves near the top of the lupine a waxier appearance by adjusting specular highlight coefficient and specular scale of the surface material. Bump mapping gives the leaves a slightly wrinkled appearance. The height of the simulated bumps produced by bump mapping is gradually decreased as we move upward along the plant. The material properties for the flowers have been similarly adjusted according to positional information. The rendering instructions for one of the leaf materials generated by the L-system is shown in Figure 4.8.

Figure 4.7: Lupine. Rendering properties such as color, specularity, and bump mapping are controlled through the use of material modules.

Algorithm 2 A snippet from the lupine L-system, illustrating the use of the shade tree in Figure 4.6 to construct materials. The leaf rendering parameters are based on the leaf's distance from the base of the plant.

1. Leaf($relativeDistance$): $0 \leq relativeDistance \leq 1$
2. {
3. $r = \text{func}(\text{RED}, relativeDistance)$;
4. $g = \text{func}(\text{GREEN}, relativeDistance)$;
5. $b = \text{func}(\text{BLUE}, relativeDistance)$;
6. $bumpiness = 2.3 - 2 \times relativeDistance$;
7. $coefficient = 20 - relativeDistance \times 18$;
8. $specular\_scale = 0.2 + 0.8 \times relativeDistance$;
9. } $\longrightarrow$
10. @Mt("*material*", "%*m*", "%*m*")
11. @Ms("*bumpmap*", "%*m*", "%*m*")
12. @Ms("*texture_bumpmap_normal*", "*bumpy.png*", 3, *bumpiness*, 1)
13. @Ms("*phong*", $0, 0, 0,$ $r, g, b,$ "%*s*", $coefficient$, $specular\_scale$)
14. @Ms("*shadow_scale*", $0.2, 0.25, 0.2$)
15. ...

4.7 Implementation

An outline of the implementation of dynamically generated materials in CPFG is pictured in Figure 4.9. When CPFG is run, it generates graphical output for a target rendering system, whether it be a realtime system (OpenGL) or an offline system (Dali, Rayshade, Renderman, etc.). CPFG must provide the instructions for generating new materials in the the target rendering system.

An L-system file describing a plant model along with material specifications is given to

```
#define material material_107 {
   surface "bumpmap" {
      "bump" "texture_bumpmap_normal" {
         "texture" "bumpy.rgb",
         "project" 3,
         "bump_scale" 2.188,
         "wrap" 1
      },
      "shader" "phong" {
         "ambient" 0 0 0,
         "diffuse" 0.663296 0.708069 0.079677,
         "specular" 0.18 0.27 0.15,
         "coefficient" 18.992
         "specular_scale" 0.2448
      }
   }
   shadow "shadow_scale" {
      "scale" 0.2 0.25 0.2
   }
}
```

Figure 4.8: One of the leaf materials generated for the Dali renderer by Algorithm 2. The material is for a leaf near the base of the plant (*relativeDistance* in the algorithm is 0.056).

---

the *L-system string generator*. The resulting string of modules must then be sent through the *L-system string interpreter*, which parses each module and its parameters. When the string interpreter encounters a material or sub-material module, it reads the shader name from the first parameter and checks for the corresponding shader description in the shader file. If the shader description's list of renderers does not include the the target rendering system, the module is skipped; otherwise, a material object is generated.

The *material object* is a collection of variables corresponding to the appearance parameters from the shader description. The variables are assigned the values provided by the module's parameter list. Shade trees can be generated by making variables point to other material objects.

The material object is then sent to the *rendering interpreter*. This interpreter implements the turtle dispatcher interface (see Section 2.4) and generates the instructions for the

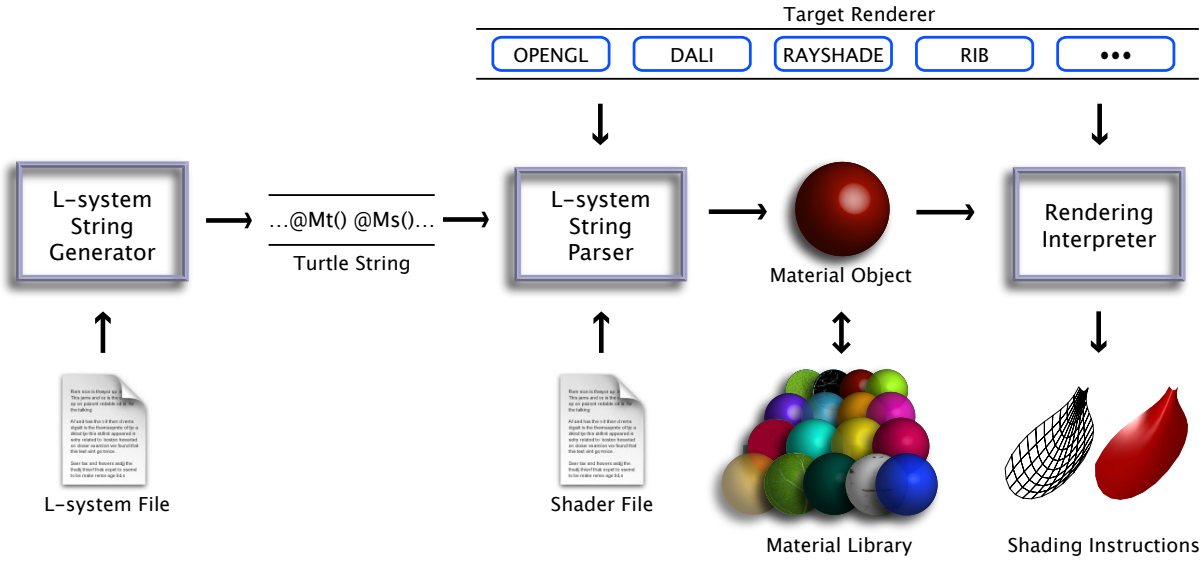

Figure 4.9: Implementation of dynamically defined materials in CPFG

target rendering system. The "create material" function in the turtle dispatcher interface is called. This function must use information in the material object to generate shading instructions for the renderer. If CPFG is rendering to OpenGL, these instructions will consist of "glMaterial" function calls. If it is rendering to an offline system, the instructions will be written to a file conforming to the renderer's specifications. Finally, the surface of the model can be shaded with the new material.

The material object can optionally be compared against a library of all previously generated materials. If the material does not exist in this *material library*, it is added to the library and a new material is generated by the rendering interpreter. If the material already exists, no new material is generated and the string parser moves on to the next module. This feature is useful to prevent redundant material definitions for rendering interpreters that output a rendering file. Suppose that a production containing a material module with constant parameters is repeatedly called. Normally, the rendering interpreter will write a new, albeit redundant, material description to the file for each material module. By using a material library, we ensure that the material is only written once.

Whenever support for a new rendering system is added to CPFG, the "create material" function in the new rendering interpreter must be implemented. CPFG can currently render to several offline systems, but only supports one real-time system (OpenGL), and does not make use of real-time shaders. Future work would involve selecting real-time shaders via material modules to change the appearance of a real-time rendered plant.

Chapter 5

Illuminating and Shading Plants

The appearance of plants is influenced by light from the environment passing through and reflecting off their soft tissues. Paying insufficient care to illumination and shading of plant models will result in tissues that appear hard and opaque, as well as shadows that appear excessively dark. In this chapter, a simple BDF (Bidirectional Distribution Function) shader that captures proper light interactions on leaves and petals is developed. The shader takes into account translucency and differences in reflectance and transmittance values for opposite sides of leaves. Global illumination ensures that plant surfaces receive reflected and transmitted light from nearby surfaces. By surrounding a plant model with a hemispherical light source, illumination from the sky may also be simulated.

5.1 Light Scattering in Leaf Layers

A magnified cross-section of a leaf blade reveals a relatively thick photosynthetic region, known as the *mesophyll*, sandwiched between thin, protective layers of epidermal cells [84, 101] (Figure 5.1). Both the upper and lower layers of epidermal cells (the *adaxial epidermis* and *abaxial epidermis*, respectively) are covered on their outside by a waxy coating, responsible for specular reflection. The epidermis layers are transparent and allow light to pass through to the mesophyll, which is composed of two layers. Beneath the adaxial epidermis is a layer of elongated, highly-diffusing palisade cells, responsible for much of the scattering of light that enters a leaf. Just above the abaxial epidermis lies a spongy layer consisting largely of air space.

This collection of layers has directly influenced rendering strategies for leaves. Baranoski and Rokne [4] performed an exhaustive physically-based simulation of light scattering

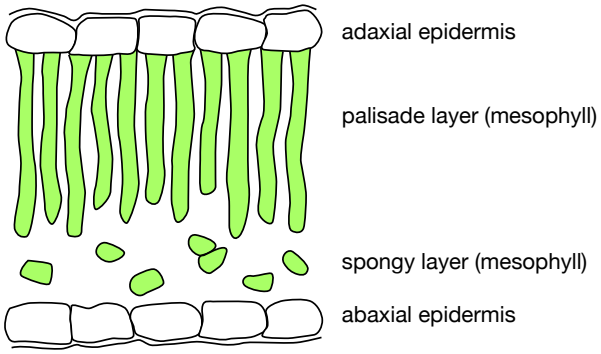

Figure 5.1: Cross-sectional view of a leaf blade (based on Figure 1a of [4]).

through layers using empirical data such as pigment concentration and cell shape. They subsequently approximated much of the scattering using pre-computed scattering profiles [5], substantially reducing computation times. Franzke and Deussen [23] represented each of the leaf layers as a texture and computed a single scatter term [38], noting that multiple scattering in thin tissues such as leaves can be adequately approximated by a small ambient factor.

Although a physical simulation of light scattering in leaves was not performed in the work in this thesis, attention was directed at capturing the effects of scattering at a phenomenological level. A simple BDF treatment of leaves and petals based on empirical observations can produce convincing renderings. The light interactions that must be captured by a BDF shader will be discussed in the following sections.

5.2 Diffuse and Specular Reflectance

Reflectance refers to the fraction of incoming light that is reflected from a surface. Reflectance of leaf surfaces has both diffuse and specular characteristics [101]. Specular highlights occur on the waxy coating of the epidermis, and typically have high reflectance values, resulting in leaf surfaces that appear nearly white (assuming a white light source), especially at grazing angles [30]. Irregularities on the leaf surface, such as veins and bumps,

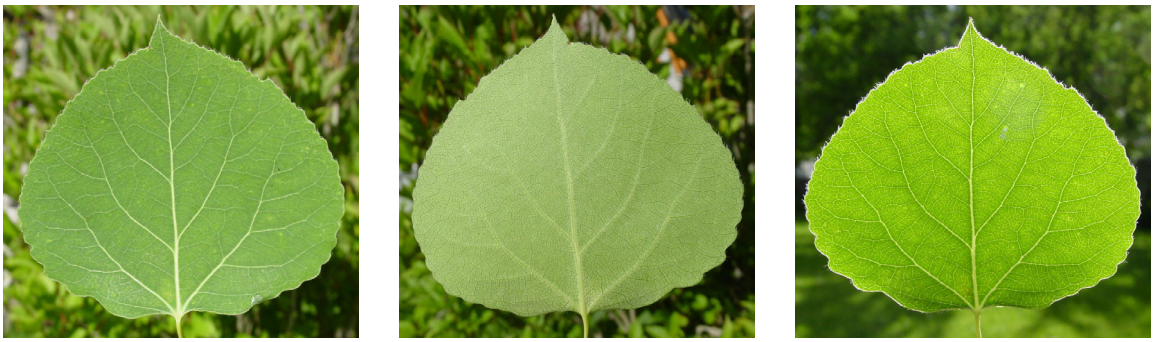

(a) (b) (c)

Figure 5.2: Front (a) and back (b) surfaces of a frontlit poplar leaf. Notice the paler appearance of the backside. A backlit poplar leaf with its front surface visible (c) has a large transmittance, compared to the reflectance for frontlit leaves.

---

may cause specular highlights to break up across the blade. In a Phong-based leaf shader, highlights can be controlled with a specular power coefficient (e.g. low coefficient values generate broad highlights for waxy leaves). Bump maps are used to simulate surface irregularities.

Light that scatters in the mesophyll and re-emerges from the leaf surface exhibits diffuse, Lambertian characteristics. Diffuse reflectance tends to be considerably lower than specular reflectance, since scattered light may pass straight through to the other side of the leaf or become absorbed by the mesophyll's photosynthetic cells. The back surfaces of leaves usually appear paler than the front (Figure 5.2), because large air gaps in the spongy layer adjacent to the back surface reflect most light before it has a chance to scatter among the pigmented cells of the mesophyll [101]. The leaf shader presented in this thesis distinguishes between the front and back sides of a leaf surface so that relative brightness may be accordingly adjusted. If the front and back appearance of leaves varies dramatically, the shader supports two separate leaf colors (or texture maps) as well.

Diffusely reflected light from a strongly pigmented surface such as a bright red petal may travel to neighbouring leaves and petals, influencing their coloration. This subtle phenomenon is known as color bleeding, and was first simulated with radiosity methods

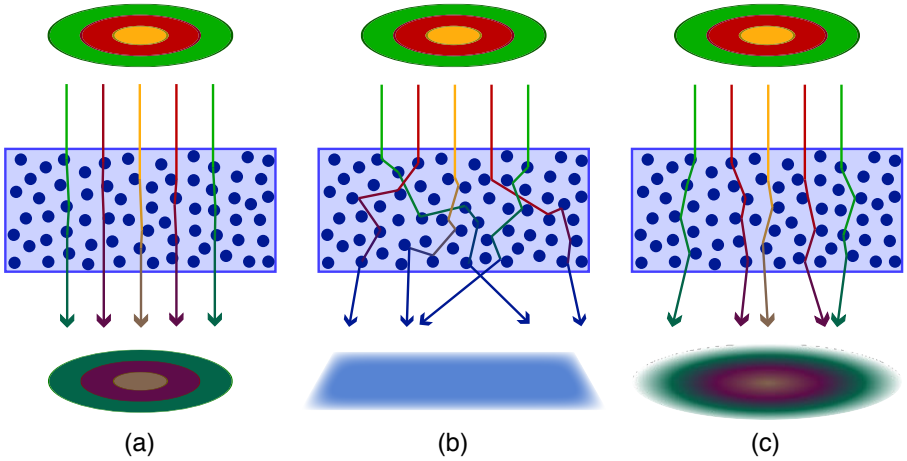

Figure 5.3: Varying degrees of scattering directly affect the passage of light through materials and influence how we perceive obscured surfaces. (a) Transparency: Particles in the material do not scatter photons, so light rays follow straight paths and transmit a sharp image of the hidden surface. (b) Translucency: Particles in the material are highly scattering and incoming photons follow variable paths with numerous particle collisions. Hidden surfaces are no longer visible. (c) Fuzzy translucency: Photons are partially scattered, resulting in a fuzzy projection of the hidden surface.

---

[29], but it can be simulated using distribution ray tracing as well. Color bleeding can be observed among the sepals and stamens of the trillium model in Figure 6.14.

5.3 Translucency

Materials that permit light to pass through them, without revealing surface details of the light source, are said to be *translucent*. A sheet of paper held against a lamp is translucent, because one can see the light through the paper without actually seeing the lamp. Scattering of light in a material is responsible for translucency: the scattered light can easily be seen, but any sharp details carried by the light rays are largely or completely obliterated through interactions with the material's particles (Figure 5.3). Using wave theory, collisions with particles results in a decrease in the amplitude of waves of particular wavelengths, producing a change in the color of the light. As the number of collisions increases, the color of a light ray increasingly matches the appearance of the material, and

Figure 5.4: Leaf rendered with frontlighting and backlighting. Specular highlights only appear on the frontlit surface, and the backlit surface appears more emissive due to the greater transmittance than reflectance value for leaves.

---

any resemblance to the appearance of the object or light source the ray originally left is lost. If the particles are highly scattering, light emerging from the translucent material has a diffuse nature. Without any scattering, translucency reduces to transparency, whereby light passes through a surface in a straight path, producing a sharp image. Interactions with particles in the transparent surface may still result in light attenuation and tinting of the light's color (e.g. sunglasses).

Most leaves and petals are translucent due to the scattering of light in the mesophyll as light passes from one side of a surface to another. *Transmittance* refers to the fraction of incoming light that is transmitted through a surface. Transmittance values for leaves are typically higher than reflectance values [101], with the interesting consequence that leaves usually appear brighter when backlit than when frontlit (Figure 5.2). The increased interaction of light with the mesophyll layer gives some backlit leaves a more deeply saturated surface color. Our leaf shader simulates these effects by adjusting the value and saturation of diffuse color under frontlighting and backlighting. The diffuse nature of transmitted light means that backlit surfaces do not exhibit specular highlights, so specular calculations may be ignored in that case (Figure 5.4).

5.3.1 Shadows

A shadow cast by a translucent surface is only partially darkened, in part because of reflected light from the surrounding environment, but more importantly because of transmitted light passing through the surface. Having interacted with surface's material, this transmitted light may even lend the shadow a slight tint. This effect is similar to color bleeding, with the small difference that transmitted rather than reflected light is affecting the coloration of nearby surfaces. The plant renderings in this thesis employ a shadow shader which modifies the behaviour of shadow rays that sample the light sources. Rather than completely blocking incoming radiance from a light source when a shadow ray hits a surface, radiance can be scaled by a factor equivalent to the surface's transmittance. Thus, a shadow ray passing through a surface with a transmittance of 0.5 will generate a semi-dark shadow. If the shadow ray passes through multiple surfaces, then the scaling of the incoming radiance is cumulative for each surface.

This approach to shadow calculations is an approximation, as shadow rays travel in a straight line, while attenuated light traveling through translucent surfaces in nature is usually scattered. As a result, when using the shadow shader, light passing through several surfaces results in layered shadows with visible outlines for each of the surfaces. The same situation in nature usually produces a blended shadow with uniform appearance.

When viewing a backlit surface, it is often possible to see shadows projected onto the surface from behind. This is evident, for example, in the photo of a poppy in Figure 5.5a. These backlit shadows provide a strong visual cue as to the incoming direction of the illumination. A rendered image of the backlit poppy is shown in Figure 5.7. Note that stamen shadows in the rendering are visible through two layers of petals, while the shadows in the photo are only visible through one layer. This difference in appearance is the result of the shadow ray approximation used by the shadow shader.

(a) (b)

Figure 5.5: Translucency in nature. (a) Backlit shadows on the petals of a poppy. (b) Fuzzy translucency can be observed where thin, semi-transparent petals overlap.

5.3.2 Fuzzy Translucency

If a leaf or petal is transparent enough for transmitted light rays not to scatter completely, it becomes possible to see partial details of obscured surfaces (Figure 5.3). In this thesis, this phenomenon is referred to as *fuzzy translucency*, to distinguish it from translucency where scattering is complete and no details are visible through the blade. The flower petals in Figure 5.5b exhibit fuzzy translucency. The effect is subtle, and is easily overpowered by specular highlights or if adjacent petals lie too far apart.

To simulate fuzzy translucency, a physically-based shader would trace the paths of photons as they travel through a material and collide with particles. Because this process is computationally expensive, our leaf shader achieves the same visual effect using distribution ray tracing [14]. When a ray passes through a translucent surface, secondary rays distributed about the main ray are spawned to gather radiance within a conical region behind the surface. The opening angle of the cone controls the amount of fuzziness. Small angles focus the secondary rays within a narrow region, resulting in more distinct images visible through the surface. Larger angles result in radiance from a wider region being

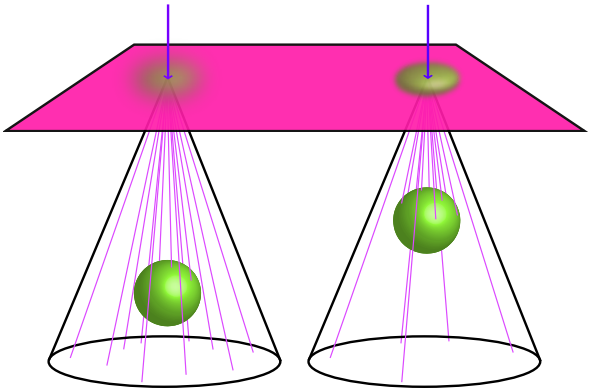

Figure 5.6: An object located far from the translucent surface will receive fewer samples and appear fuzzier than an object close to the surface.

sampled and averaged, and fuzzier images are generated. The distance between the surface and sampled objects also affects the amount of fuzziness (Figure 5.6). Care must be taken if the cone intersects with the surface, a common occurrence when the translucent ray has a large angle of incidence. In this case, radiance samples must only be taken in the region of the cone on the backside of the surface.

The frontlit poppy in Figure 5.7 has been rendered with fuzzy translucency. The relatively large distance between the translucent petals and the stamens results in fewer stochastic samples hitting the stamens. Consequently, the stamens are particularly fuzzy and only barely visible through the front petal.

5.4 Sky Illumination and Light Penetration

In a daylit environment in nature, a plant is not only illuminated by direct sunlight, but also by reflected or transmitted light from the ground and neighbouring objects, and by scattered light from the sky. If the sun is hidden by overhead branches or an overcast sky, the plant may be entirely illuminated by indirect, scattered light. This type of light arrives from all directions, producing indistinct shadows and penetrating into concealed regions of a plant (Figure 5.8).

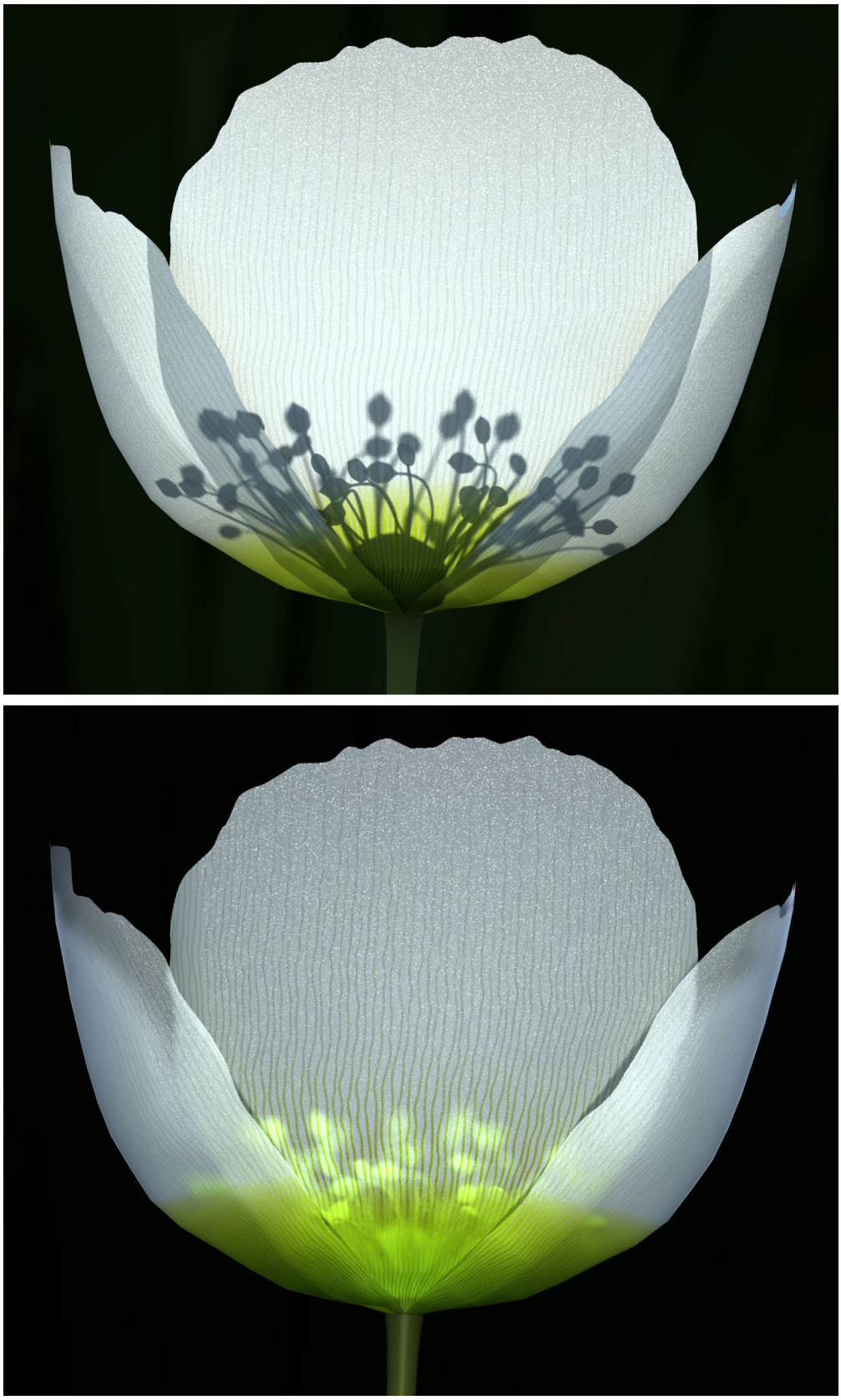

Figure 5.7: Rendered poppies with backlighting (top) and frontlighting (bottom). Stamens and obscurred portions of the central petal are visible via backlit shadows and fuzzy translucency.

Figure 5.8: Photo of a lilac without a direct source of illumination. Shadows are indistinct and the interior of the lilac gets progressively darker.

Various approaches to illumination have been used for plant models. A single area light source (representing, for example, the sun) may be used to illuminate a plant and generate soft shadows. However, single light sources produce a headlight effect, illuminating one side of the model only. Indirect illumination has often been approximated using an ambient term [72], which provides a constant basal illumination value for all surfaces. The ambient term, however, fails to capture variations in indirect illumination, causing surfaces in shadow areas to appear flat. Alternatively, multiple light sources can be placed around the object, but this creates the risk of producing several distinct shadows.

A better solution is to use hemisphere lighting, a technique with roots in environment mapping [7, 62]. Hemisphere lighting involves the placement of an emissive hemisphere around the model. Any rays that miss nearby objects while sampling their surroundings for indirect light will end up sampling the hemisphere. The radiance collected by a ray is directly proportional to the hemisphere's brightness at the sample point [16].

Using hemisphere lighting in conjunction with a spherical light source provides a basic daytime model of the sky, and greatly improves the illumination of plants [83] (Figure 5.9).

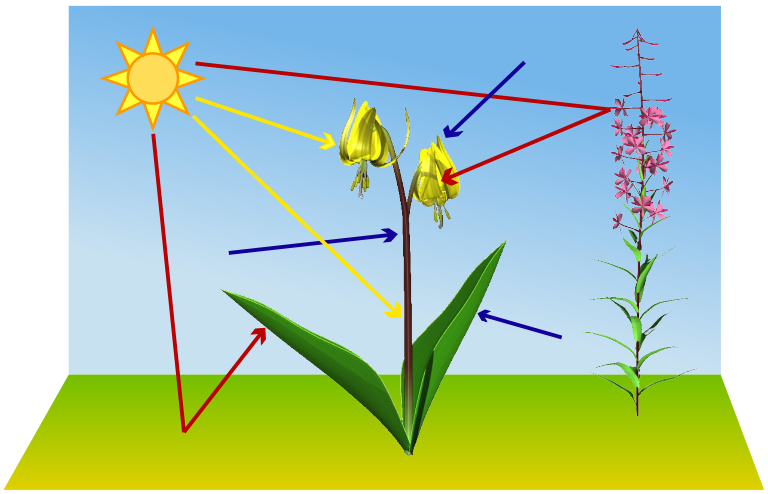

Figure 5.9: Illuminating a plant model in daylight conditions. The model is illuminated by light arriving directly from a spherical light source representing the sun (yellow arrows), and also by reflected light from the ground and neighbouring objects (red arrows) and by scattered light from the sky (blue arrows).

Light arriving from the simulated sky penetrates into shaded regions of the plant. This light penetration is further enhanced by taking into account interreflected light between surfaces, as per a full global illumination simulation. In this research, point samples from photographs of the sky have been taken to determine the coloration of the hemisphere lighting. Alternatively, color values that take into account turbidity due to haze or smoke may be computed [73]. Illumination on an overcast day can be simulated by removing any direct light sources and employing a hemisphere with a solid shade of gray. This allows us to capture the same soft, indistinct shadows seen in nature.

Figure 5.10 displays several images of lilac inflorescences rendered under various lighting conditions and with different material settings, recorded in Table 5.1. Traditional ray tracing, taking into account direct illumination only, was used for the top two lilac images. The position of the spherical light source above and to the right of the lilac results in very dark shadows, obliterating most of the model (Figure 5.10a). An ambient constant term was used to simulate global illumination in Figure 5.10b, brightening the shadow areas. However, these shadow regions appear uniform, as variations in reflected and transmitted

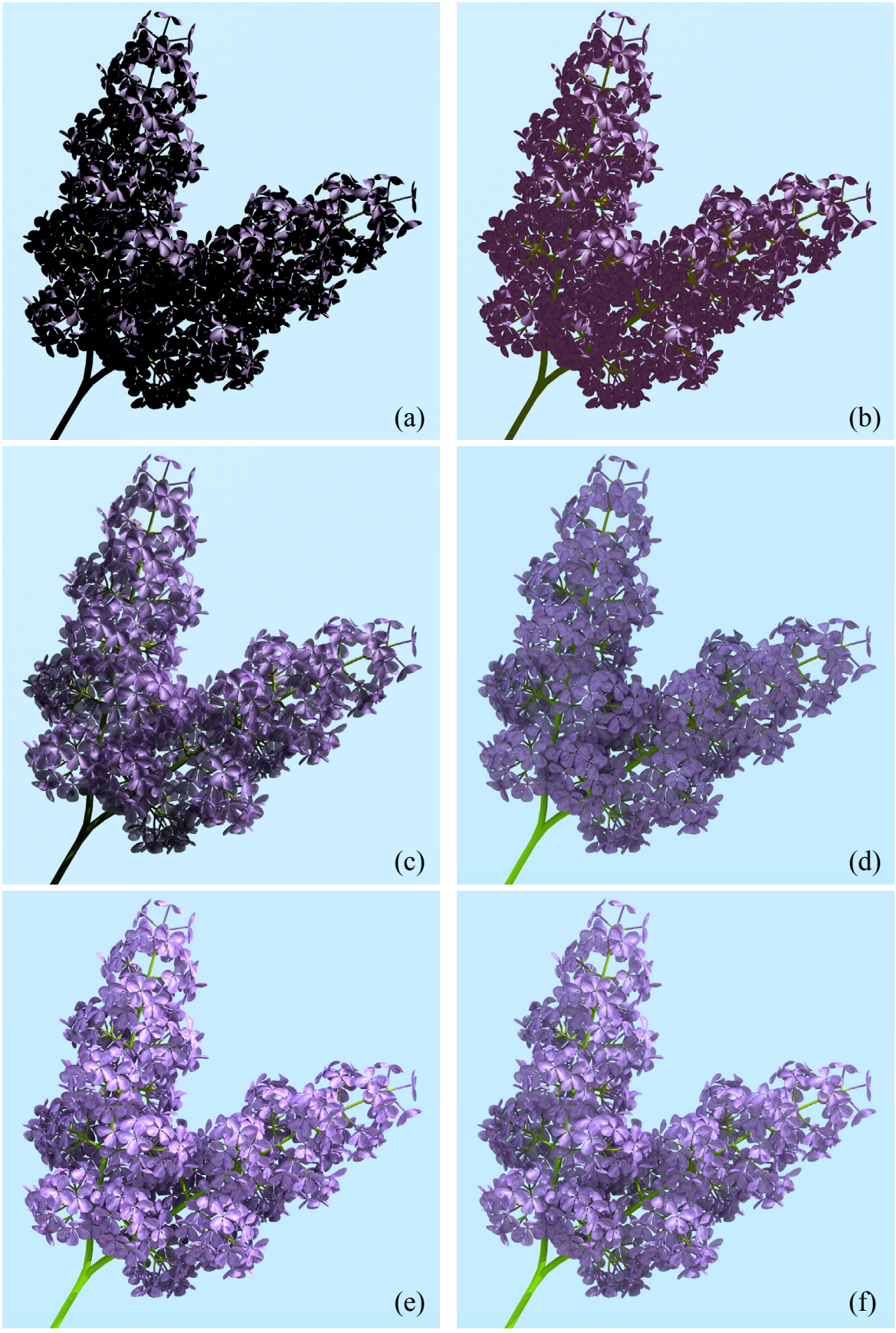

Figure 5.10: Lilac inflorescences. Refer to Table 5.1 for rendering settings.

Figure	Global Illumination	Sphere Light	Skylight	Translucency	Transparency	Cone Angle
5.10a	no	yes	no	0	0	0
5.10b	no (ambient term)	yes	no	0	0	0
5.10c	yes	yes	no	0.8	0.25	15
5.10d	yes	no	yes	0.8	0.25	15
5.10e	yes	yes	yes	0.8	0	0
5.10f	yes	yes	yes	0.8	0.25	15

Table 5.1: Illumination and translucency settings for lilac. The translucency settings are based on the leaf and petal shader appearance parameters in Figure 5.11.

illumination are not captured.

Details in the shadow regions are noticeably improved in the remaining images, where full global illumination has been applied. The petals in Figure 5.10c exhibit slight transparency and fuzzy translucency, allowing radiance from the spherical light source to penetrate into the interior of the model. The lilac in Figure 5.10d is illuminated solely by skylight, resulting in non-distinct shadows and a gradual falloff in the amount of light reaching interior regions. The lilacs in Figures 5.10e and 5.10f are illuminated both by a spherical light source and skylight, with fuzzy translucency for petals turned off in the former case.

5.5 A Leaf and Petal Shader

In this section, the leaf and petal BDF shader developed during this research is described. The appearance parameters for the shader are listed in Figure 5.11. The shader is based on the Phong illumination model [72], and includes parameters for diffuse color, specular color, and specular power (the coefficient for controlling the size of the specular highlight). The value and saturation parameters are used to change the respective properties for diffuse color, based on an HSV (hue/saturation/value) color space [39], in order to simulate differences in color intensities under frontlighting and backlighting (as in Figure 5.4).

Two important parameters are translucency and transparency, which are used to de-

Figure 5.11: Leaf BDF shader description.

scribe the scattering of light in the mesophyll. In a physically-based BSSDF shader, scattering would be simulated based on physical principles taking into account experimentally measured values for scattering and absorption terms [38, 37]. In this thesis, we simulate translucency using two approaches: fully scattered light is simulated using Lambertian reflection, and partially scattered light (required for fuzzy translucency) is simulated using the distribution path tracing approach described in the previous section. The translucency term effectively weights the contribution from the former approach, while the transparency term (together with a cone angle parameter) weights the contribution from the second approach. This separate treatment of translucency and transparency terms is often used in shaders that treat light scattering at a phenomenological level [91].

The translucency parameter controls the amount of fully scattered light that can pass through a surface. Conceptually, this scattered light interacts with the material's particles, and illuminates the surface with a user-specified diffuse color. A translucency parameter of 0 means that no scattered light can pass through the surface, and any backlit surfaces will appear completely dark. A translucency parameter of 1 results in fully illuminated backlit surfaces.

The transparency term indicates how much non-scattered light passes through a surface, thereby permitting objects behind the surface to be visible. Setting transparency and translucency terms to values between 0 and 1 results in blending of the transmitted image

Algorithm 3 Outline for a BDF shader that supports fuzzy translucency. Appearance parameters of the shader from Figure 5.11 are written in sans serif. Notationally, $*$ represents component-wise multiplication of RGB vectors and $\cdot$ represents scalar multiplication.

1. function leaf_BDF($\vec{r}$, x ,$\vec{n}$, light_sources)
2. for every light in light_sources
3. $\vec{\omega}$ = light position $- x$
4. if (surface is illuminated from front)
5. $L_r = L_i *$ diffuse $*$adjust(saturation,value) $\cdot\ R_d(\vec{\omega}, \vec{n}) \cdot (1-$transparency$)$
6. $L_r = L_i + L_i *$ specular$\cdot R_s(\vec{\omega}, \vec{r}, \vec{n})^{specular_power}$
7. else
8. L_t = light intensity $*$ diffuse $\cdot T(\vec{\omega}, -\vec{n})\cdot$translucency$\cdot(1-$ transparency$)$
9. end if
10. $L_{direct} = L_{direct} + L_r + L_t$
11. end repeat
12.
13. $L_{indirect\_front}$ =sampleRegion($\vec{n}$, 180,samples)$*$diffuse $\cdot(1-$transparency$)$
14. $L_{indirect\_back}$ =sampleRegion($-\vec{n}$, 180,samples)$*$diffuse $\cdot(1-$transparency$)\cdot$translucency
15. L_{fuzzy} =sampleRegion($\vec{r}$, cone_angle, samples)$\cdot$transparency$\cdot$translucency
16.
17. $L = L_{direct} + L_{indirect\_front} + L_{indirect\_back} + L_{fuzzy}$
18. end function

of hidden objects and the surface's diffuse color. To make these objects appear fuzzy, the light rays must be partially scattered, and a cone angle term is required to permit stochastic sampling within a conical region. Used together, the parameters for translucency, transparency, and cone angle provide full control over the appearance of translucent leaves and petals.

Algorithm 3 illustrates the basic implementation of the leaf and petal shader. In ad-

dition to the property values specified by the user, the BDF shader requires the direction of the incoming sampling ray $\vec{r}$, the intersection point x of the ray with the material, the surface normal $\vec{n}$, and an array of light sources that provide direct illumination (line 1).

The shader begins by determining the radiance contribution from each of the light sources. This contribution is computed from a BRDF if the light source is positioned in front of the surface, or from a BTDF if the light is behind the surface. For frontlighting, the diffuse contribution of the light is computed in line 5. The function *adjust* modifies the saturation and value (i.e. brightness) of the surface by scaling the RGB components of the diffuse color. As observed in Figure 5.2, the saturation and brightness of the diffuse color are lower under frontlighting than under backlighting. The product of diffuse color and light intensity is weighted by R_d, the diffuse reflectance function. In this work, a simple Lambertian function was used for R_d:

$$R_d(\vec{\omega}, \vec{n}) = \vec{\omega} \cdot \vec{n}$$

where $\vec{\omega}$ is the normalized direction to the light source. A more comprehensive implementation of the shader could make use of empirical reflectance profiles, such as those provided in [101], to compute R_d. Line 5 also scales radiance by $(1 - transparency)$, as materials reflect less light as they become increasingly transparent. Line 6 computes the specular contribution of the light using the specular reflectance function R_s:

$$R_s(\vec{\omega}, \vec{r}, \vec{n}) = (2\vec{n}(\vec{n} \cdot \vec{\omega}) - \vec{\omega}) \cdot \vec{r}$$

derived in [21], and raised to the power of the specular power coefficient. The specular contribution is not affected by the transparency parameter, since specular reflections occur on the waxy surface of a leaf or petal rather than in the mesophyll.

For a backlit surface, the diffusely transmitted light is computed in line 8. The transmittance function T computes transmittance assuming a fully translucent surface, and is then scaled by the actual translucency parameter. In this work, T is based on the same

Lambertian function used for diffuse reflectance R_d. Finally, the radiance must once again be scaled by $(1 - transparency)$, to account for the visibility of hidden objects that may be seen through the surface.

Next, indirect light contributions are computed (lines 13 - 15). Path tracing is used to stochastically sample the surroundings for incoming radiance. A cone centered around a particular direction vector is used as the sampling region. The shader's *samples* parameter indicates how many times the region is sampled. Indirect radiance is gathered from the front side of the surface in line 13. An opening angle of 180 degrees centered about the surface normal effectively sets up a hemispherical sampling region. Indirect radiance from the back side of the surface is similarly computed in line 14, except that the sampling region is centered around $-\vec{n}$, and the radiance is scaled by the surface's translucency.

Line 15 computes the radiance contribution due to transparency, allowing objects behind the surface to be seen. The region behind the surface is stochastically sampled around $\vec{r}$ using *cone_angle* as the opening angle, in order to produce the fuzzy translucency effect.

Finally, line 17 sums up the radiance due to direct and indirect illumination for point x on the surface.

Chapter 6

Texturing Surfaces

Texturing is an important facet of realistic rendering, significantly increasing the amount of detail visible on a model. This chapter discusses the texturing of generalized cylinders, and introduces several procedural methods for generating textures, particularly venation patterns.

6.1 Setting up Texture Space

Texture mapping [11, 7] is a common computer graphics technique to create the illusion of complexity on an otherwise barren surface. A *texture map* is a rectangular digital image of the desired surface appearance. The map has *texture coordinates* u and v, ranging from 0 to 1 along the image's width and height respectively. The texture is mapped onto an object by associating points on the surface of the object with points in the texture space. This mapping from 3D space to 2D space ($R^3 \rightarrow R^2$) requires that a 2D parameterization of the object's surface be found.

The following sections examine some of the methods that have been used for texture-mapping various surfaces used in L-system modeling, and introduce a modified method for computing texture coordinates on generalized cylinders.

6.1.1 Tileable versus Non-Repeating Textures

Some types of textures prepared for plant surfaces are *tileable*. Stems and branches have traditionally made use of tileable textures for bark [8], since many bark patterns have a semi-repetitive nature. The texture's edges must be specially prepared so that there are no visual discontinuities along seams during tiling. More recently, synthesis of bark

patterns [49] made it possible to map continuous, non-repeating textures exactly once along a generalized cylinder. Leaves, petals, and sepals usually require a single texture that fits the entire surface [8, 54], since features such as venation patterns and petal markings do not tile well.

6.1.2 Fitting Textures on Bezier Patches

Leaf and petal surfaces are often modeled as Bezier patches that can be referenced and manipulated by L-systems [31, 76]. The parameter space of a Bezier patch has a uv domain ranging from 0 to 1, making it straightforward to map parameter space into texture space and obtain a precise fit.

A Bezier patch produces a smooth surface whose overall shape is adjusted by control points. On the other hand, generalized cylinders are built segment by segment during L-system interpretation, so they can be freely shaped and moulded at every step. In conjunction with positional information [82], generalized cylinders provide a powerful modeling alternative to Bezier patches. It is therefore important to consider texture mapping of generalized cylinders as well.

6.1.3 Tiling Textures on Generalized Cylinders

Generalized cylinder surfaces have often been parametrized for texture-mapping purposes [8, 58, 49]. For a closed generalized cylinder, the u domain of texture space wraps around the cylinder's circumference. On an open generalized cylinder, the u domain is stretched transversely across its surface. In either case, the v domain is stretched along the cylinder's axis, with v coordinates projected out onto the cylinder's surface.

If a texture is to be tiled along a cylinder, the v domain repeats at regular intervals until the end of the cylinder is reached. The v coordinates may be computed as follows:

$$v = Dec(aR) \tag{6.1}$$

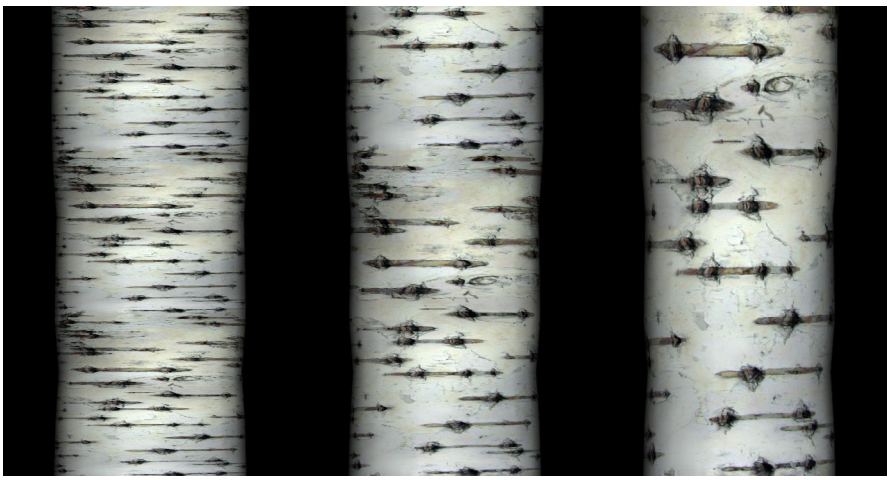

Figure 6.1: Tiling a bark texture on a trunk. The aspect ratio of the texture can be adjusted with R.

The various parts of this equation are explained below:

- The value a is the length of the generalized cylinder axis. After the nth segment of a cylinder, a has a value of:

$$a_n = \sum_{k=0}^{n} A_k \tag{6.2}$$

  where A_k is the axis length of segment k (see Figure 2.3).

- The *aspect ratio* R describes the height-to-width ratio of the texture as it is stretched across the surface. Increasing the aspect ratio stretches the texture along the axis of the cylinder (Figure 6.1), while decreasing the ratio squishes the texture.

- The function $Dec()$ returns the fractional portion of the argument, thereby enforcing a range $0 \leq v < 1$.

In order to hold the aspect ratio of image pixels on the surface constant as the width of the cylinder changes, the calculation may further take into account the cylinder segment's circumference [8, 58]. For example, when tiling a bark texture on a cylinder that decreases in width, values of v should increase more rapidly so that the texture doesn't appear to elongate.

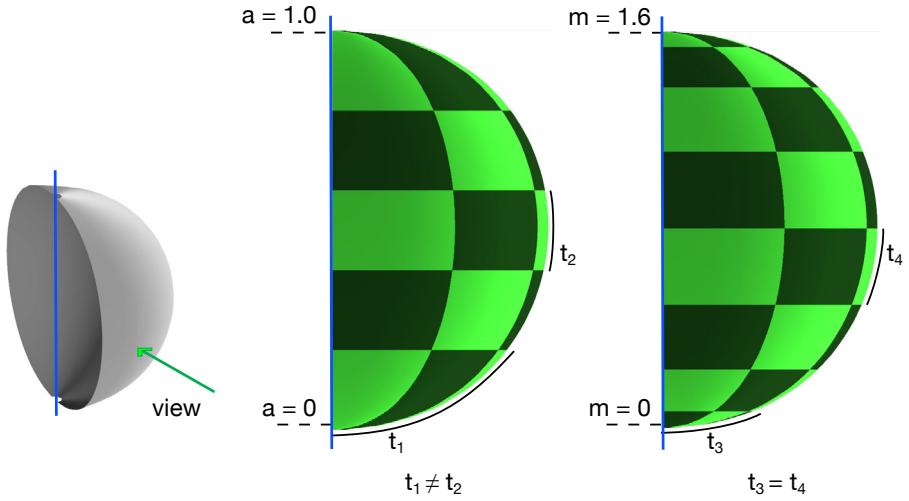

Figure 6.2: Two views of a texture-mapped semi-sphere built from an open generalized cylinder. The height of each checkerboard tile represents a 0.2 increment in the value of v. In the left view, texture parameters have been spaced according to turtle steps along the cylinder axis. Consequently, along the surface of the cylinder, tile t_1 covers a larger distance than tile t_2. In the right view, texture parameters are computed based on surface distance. Tiles t_3 and t_4 cover the same distance. Textures mapped onto the right cylinder will be stretched uniformly across the surface.

6.1.4 Fitting Textures on Generalized Cylinders

Non-repeating textures for organs such as leaves, stems, and petals modeled with generalized cylinders need to fit exactly once across the entire surface. As before, texture coordinates need to be generated for the cylinder segments, but in this research, the method has been slightly modified, after taking into account two considerations.

Distortion

Leaf and petal textures tend to have a symmetric composition along a central vertical axis. A texture for a dicot leaf, for example, is divided into two halves by the central primary vein. When mapping these textures onto a generalized cylinder, it is desirable to limit distortion of the texture by mapping its central axis uniformly along the central longitudinal arc of the cylinder surface. The traditional method of basing the v domain of texture space on the length of the cylinder axis means that textures will experience excess

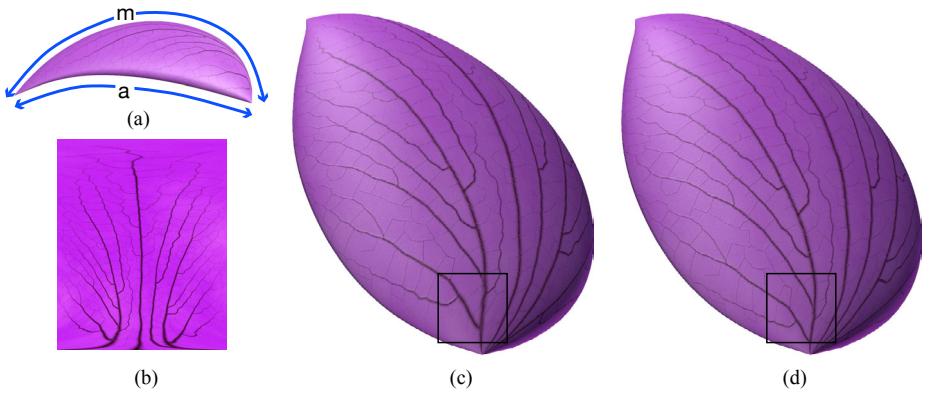

Figure 6.3: Texture mapped petal. (a) View of the petal from the side, with mid-arc m and axis a of the generalized cylinder illustrated. The texture map is shown in (b). The v domain of texture space on the petal in (c) is stretched along a, while on petal (d) it is stretched along m. The texture is excessively stretched in (c) where the petal surface angles outward from the axis.

---

stretching if the surface angles outward from the axis (Figure 6.2).

A solution devised in this research is to compute v based on the length of the mid-arc of the generalized cylinder (see Figure 2.3). Equation 6.1 is modified as follows:

$$v = Dec(mR) \tag{6.3}$$

where m is the length of the mid-arc. The value of m after the nth segment of a generalized cylinder is:

$$m_n = \sum_{k=0}^{n} M_k \tag{6.4}$$

where M_k is the mid-arc length of segment k. Figure 6.3 compares the texture mapping of a petal based on use of the cylinder axis versus the mid-arc.

Tile Factor

Because our goal is to fit textures exactly once on the surface, we should be able to say directly that a texture is to be tiled once, rather than having to specify an aspect ratio. A *tile factor* indicates how many times a texture should be tiled along a cylinder, and is inversely related to aspect ratio.

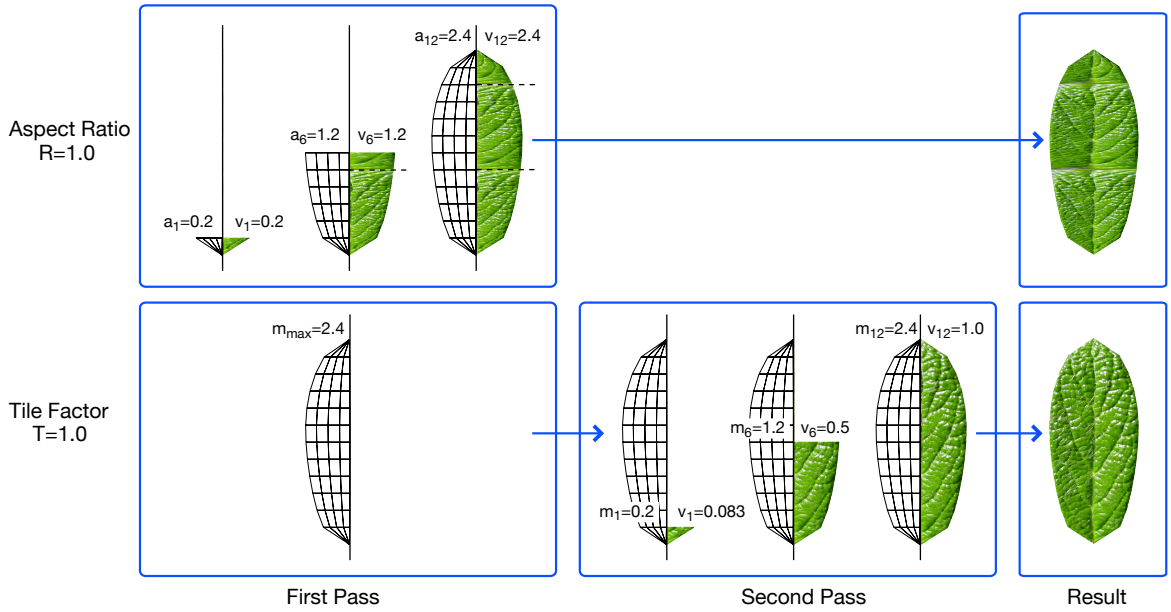

Figure 6.4: Calculation of v texture coordinates after cylinder segment n (for $n = \{1, 6, 12\}$). The leaf's generalized cylinder consists of 12 segments, each having an axis length (or mid-arc length) of 0.2 units. Coordinates for the upper mesh are computed with Equation 6.1 (one-pass approach) using an aspect ratio of 1. Coordinates for the lower mesh are computed with Equation 6.5 (two-pass approach) using a tile factor of 1.

Mapping a texture onto a cylinder a pre-determined number of times requires that the entire arc-length of a cylinder, m_{max}, is known in advance, so that the relative positions of segments in texture space can be computed. Texture coordinates for generalized cylinders in Section 6.1.3 could be computed in a single pass, but use of a tile factor requires a second pass. During the first pass, the value of m_{max} is determined once the entire generalized cylinder has been built. A second pass along the cylinder generates v texture coordinates as follows:

$$v = Dec\left(\frac{m}{m_{max}}T\right) \tag{6.5}$$

The parameter T is the tile factor, and in the case of texture fitting, is given a value of one. A visual comparison between the one-pass and two-pass approach to texture fitting is shown in Figure 6.4.

6.2 Procedural Textures

Leaves and petals display such a wide diversity of colors and patterns that many different textures are required to properly capture the desired appearance of plant models. These textures can be obtained directly from nature using flatbed scanners [54] or photographs [8], provided that flat specimens are readily available. Alternatively, an artist may create a texture from scratch, adding the exact splotches, gradients, specks, and striations seen on the real surface. These methods of generating textures can be time-consuming, especially when multiple versions of a texture are required to capture the variability of surface appearances in nature. The process of obtaining textures can be shortened by making use of procedurally generated textures to produce specific features.

Procedural textures [70, 18] are created mathematically, permitting details to be generated in a resolution-independent manner from a set of user-adjustable parameters. The texture is generated using a procedural function that accepts a set of coordinates and immediately computes a value (or set of values) for this point. The value is typically interpreted as a color, but may also be used for many other purposes, for example to perturb normals or displace surfaces. When used with 3D coordinates, procedural textures can generate solid textures such as those seen on sculpted marble [69]. In this section, we are concerned with generating details on parameterized leaf and petal surfaces, so we will use 2D procedural textures computed as a function of texture coordinates.

By building a shader around a procedural texture algorithm, it is possible to specify the texture's parameters from within an L-system using material modules. In this way, unique textures can easily be specified and generated for every single leaf or petal on a plant. Because procedural functions are able to specify a texture value for any given coordinate, this type of shader is well suited for point sampling (i.e. ray tracing). This section introduces shaders for generating translucent outlines and parallel venation patterns based on 2D functions.

Figure 6.5: Daylily leaves are rimmed by translucent edges.

6.2.1 Translucent Outlines

When illuminated from behind, some leaves and petals display a bright fringe of light along their edges. During the course of this work, the effect has been observed in two types of situations: light shining through thin, translucent tissue rimming the edges (Figure 6.5), or light scattering among short hairs or fuzz along the edges (Figure 7.1). The former case is discussed below; the latter case is covered in Chapter 7.

A trivial way to simulate translucent edges is to paint them directly onto a texture. The texture is then mapped onto a blade, and the entire surface rendered as a single material. This method is problematic, since the translucent edges have different light transmission and scattering properties than the rest of the blade. In this work, the blade is partitioned into two regions of separate materials. The edge region is rendered with a highly translucent material, while the central portion of the blade is rendered with a different material.

The edge regions typically have a constant width around the entire perimeter of the surface. Texture space can be used to define these regions. A leaf modeled as an open generalized cylinder has a varying width controlled by a function, as well as a u domain in texture space varying from zero to one, from one edge to another. An absolute width

w_{abs} for the translucent outlines can be specified and converted into a width w_{tex} in the u domain of texture space. The width of the outline in texture space varies inversely with the leaf's width function $\mathcal{F}_{width}$, so w_{tex} at a distance l along the axis of the leaf is computed as:

$$w_{tex} = \frac{w_{abs}}{\mathcal{F}_{width}(l)}$$

An outline shader handles the partitioning of a leaf blade during ray tracing (pictured as a sub-shader node in the shade tree in Figure 6.9). The shader requires parameters for outline width and the surface's width function. It returns a value of zero or one, indicating if the ray intersecting the blade hit the edge or central region, and may optionally return a value between zero and one to simulate a transition from one region to another. By passing this value to a blend shader, the appropriate materials for either region may be chosen or blended together. Figure 6.6 illustrates the outline shader at work.

Because the outline width is measured in a transverse direction along the u domain rather than perpendicularly to the edge, the outline will appear to shrink if the edge angles sharply outward from the leaf's axis (for example, at the base of a leaf where the stem joins the blade). Translucent outlines tend to be narrow strips, so shrinkage in the outline width is often visually negligible.

6.2.2 Venation Systems

One of the most striking features on leaves and petals is the venation system. Leaf and petal veins are a conspicuous component of the vascular system, which serves to distribute nutrients throughout the entire plant [26]. Procedural generation of veins is an especially attractive goal for computer graphics because of the time-consuming process of hand-modeling, scanning, or photographing multiple vein patterns for a plant model.

Many varieties of veins and vein patterns exist. These have been extensively categorized in work by Melville [60] and Hickey [34]. Individual veins belong to a particular vein *order*,

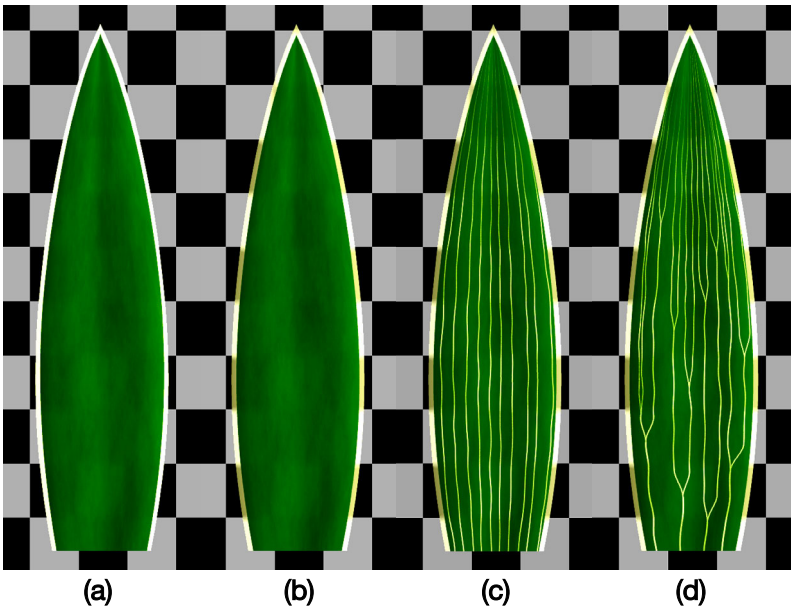

Figure 6.6: The entire surface of the leaf in (a) is a single texture map renderered with a uniform material. The edge regions and veins in the remaining leaves are procedurally generated, and use materials with different translucency properties than the rest of the blade. The checkerboard pattern is visible through the edge regions in (b) due to fuzzy translucency. Parallel venation with translucency has been added in (c) and includes branching in (d).

---

depending on their relative width and location on a blade. *Primary* or *first-order* veins are dominant veins originating at the base of a leaf. *Secondary* veins typically branch from the primary veins, and are noticeably thinner. Further branching results in *tertiary* and *higher-order* veins, which tend to form *areoles*, closed polygonal islets that often contain free-ending veins [65]. Veins of various orders are arranged in different ways depending on the type of leaf. *Monocots*, or grass-like leaves, typically display *parallelodromous* venation, with several primary veins emerging from the base and running in a more or less parallel fashion (e.g. daylily leaves in Figure 6.5). *Dicots*, or broad, stalked leaves, may also feature parallelodromous venation, but more commonly bear a *pinnate* pattern, with secondary veins emerging laterally from a single primary vein (e.g. poplar leaves in Figure 5.2). While Hickey's vein classifications have been directed primarily at leaves, similar patterns can be found on petals as well.

Various methods have been utilized to generate procedural vein patterns. Genetic algorithms have been used to construct L-systems that approximate pinnate patterns with primary and secondary veins on dicot leaves [86]. Higher order venation has been simulated using a cellular texture basis function that partitions texture space between feature line segments [10]. More recently, structured particle systems have been used to model complex venation systems [85, 88]; these will be further discussed in Section 6.2.4.

6.2.3 Ray Traced Parallel Veins

This section introduces a shader for generating parallelodromous venation. The shader is based on a procedural texture that takes advantage of the mesh's texture coordinates to generate the vein pattern. Parameters for the vein shader include the number of veins, the number of times the veins will branch, and vein width. For a set of *uv*-coordinates, the shader returns a value indicating whether a vein has been hit.

Veins in the shader are represented as binary tree structures. A *parent* vein may branch into two *child* veins. We refer to a pair of child veins as *siblings*. For any vein, it is possible to traverse the tree to find the vein's parent, sibling, or children.

During an initialization phase, the shader divides texture space into a grid of rows and columns (Figure 6.7). Each column is called a *vein region*. A single vein passes through every vein region. If the vein branches, the vein region is split into two additional vein regions, one for each child vein. Each row is called a *band*, and a new band is added every time a vein branches. A pattern with no branching veins requires only one band. If the pattern includes branching, the branch points are set at non-uniform intervals along the path of veins.

Two aspects of the vein shader will now be examined in detail: generation of the veins, and divergence of veins at the branch points.

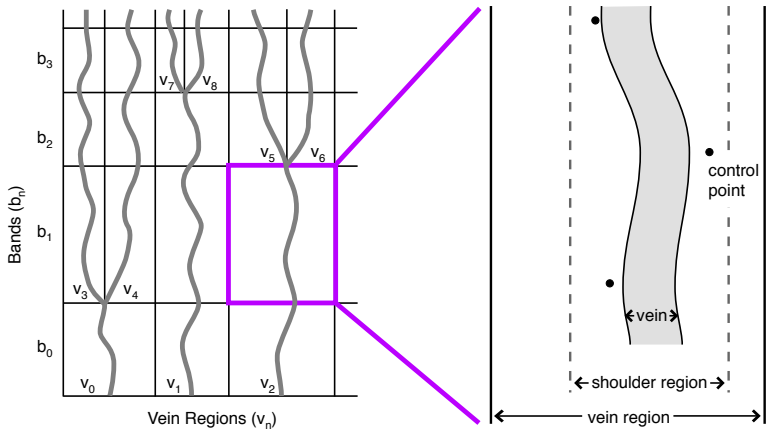

Figure 6.7: To generate parallel veins with branches, texture space is partitioned into bands consisting of rows of vein regions. A vein region contains a single vein, whose path is influenced by a series of control points lying within a shoulder region.

Vein Generation

The shader's base vein width parameter indicates the width of veins at the base of the texture. This width is gradually reduced as veins pass through the v domain toward the top of the texture. Because the width parameter is given in object space, it must be converted to a width in texture space, w_{tex}, using the same method as outlined in Section 6.2.1.

A vein has a transverse location l given as a u coordinate in texture space. The vein's lower and upper bounds are $l - \frac{w_{tex}}{2}$ and $l + \frac{w_{tex}}{2}$, respectively. Rays hitting the surface within these bounds will generate a vein.

In a straightforward implementation, the vein location is constant for the entire length of the vein, producing a perfectly straight path along the entire v domain in texture space. Veins in nature, however, usually follow a slightly wavy path. For a more natural appearance, our implementation jitters the vein location at uniform intervals of v. Each jittered point (l, v) forms a *control point*, and lies within a *shoulder region* that demarcates the path followed by the vein (Figure 6.8). By using the control points to guide an approximating spline, a vein with a smooth, wavy appearance is generated. Approximating splines with

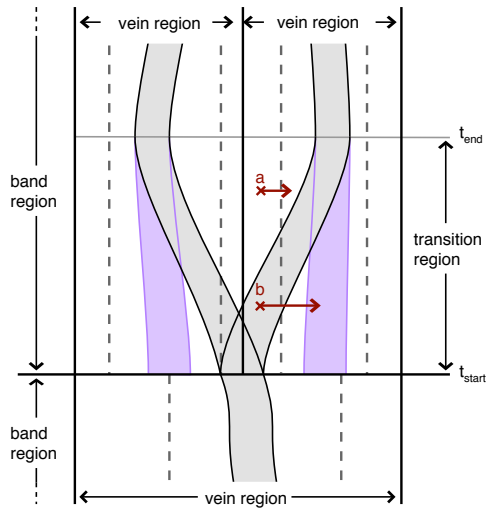

Figure 6.8: A branching point is followed by a transition region, permitting the child veins to settle into their new vein regions. Without a transition region, the child veins would continue to follow the spline paths indicated in violet.

convex-hull property ensure that the veins remain within the shoulder region. *B-splines* [6] have been used for the parallel veins in Figure 6.6.

Branching Points

When a parent vein splits into child veins, two new vein regions are produced. If the child veins are rendered without regard for the branching point, they will continue to follow their wavy spline path centered in their respective vein regions without merging together (Figure 6.8). The solution is to define a transition region which spans a portion of the v domain at the start of a new vein region. The length of the transition region determines how quickly the child veins diverge from their parent.

Conceptually, transition regions operate by shifting u coordinates in texture space of one vein region toward the vein region occupied by the sibling vein. This is achieved in practise by adding an offset to the u coordinate of any ray intersection point (u_{ray}, v_{ray}) in a transition region. The offset, u_{offset}, depends on the relative location of the intersection point within the transition region. If the intersection point lies at the start of the transition region, its u coordinate is offset by the difference between the child vein's transverse

location, l_{child}, and the parent vein's transverse location at the branching point, l_{parent}. If the intersection point lies at the end of the transition region, its u coordinate remains unchanged. For any intersection points between these extremes, the offset is weighted by a cubic polynomial that creates a smooth transition. The surface is then queried at the new coordinates $(u_{ray} + u_{offset}, v_{ray})$ to test for intersection with a vein.

Figure 6.8 illustrates the offset added to two intersection points, a and b, within the transition region. Because the offset on point a does not place the point in the violet vein path, no vein hit takes place. The offset on point b places the point directly inside the violet vein path, so a vein hit is considered to take place.

Algorithm

The function indicating if the ray intersecting the surface hits a vein is displayed in Algorithm 4. Two binary searches (lines 2 and 3) are performed using the ray intersections's texture coordinates to determine in which band and vein region the ray landed.

Lines 4 to 7 add an offset to the intersection's u coordinate if the ray landed within the vein region's transition region. The u coordinate, whether offset or not, is next compared against the boundaries of the shoulder region (line 8). If u exists outside the boundaries, the ray intersection most definitely does not hit a vein. If u exists within the shoulder region, the vein's transverse location is computed based on the spline defining the vein path (line 9). The vein's lower and upper bounds are then computed (line 10). If the ray intersecton occurs within these bounds, a vein hit is confirmed. While line 12 of the algorithm simply returns a value of 1, the implementation used for this research generates a weighted value that can be used for various purposes during rendering. For example, by returning a value of 1 for the center of the vein and increasingly smaller weights toward the vein's edges, a vein can be rendered with soft edges. As well, fading veins are rendered by returning increasingly smaller weights as the tip of a blade is approached.

The binary searches are the slowest part of the algorithm, requiring a runtime of

Algorithm 4 The algorithm used by the parallel vein shader to determine if a ray intersected a vein.

1. function hitVein(u, v)
2. currentBand = binarySearchForBand(v)
3. currentVeinRegion = binarySearchForVeinRegion(v, currentBand)
4. if v occurs within currentVeinRegion's transition region $[t_{start}, t_{end}]$
5. $x = \frac{v - t_{start}}{t_{start} - t_{end}}$
6. $u = u + (2x^3 - 3x^2 + 1) * (l_{child} - l_{parent})$
7. end if
8. if u occurs within currentVeinRegion's shoulder region
9. l_{vein} = spline(v)
10. veinBounds = $[l_{vein} - \frac{w_{tex}}{2}, l_{vein} + \frac{w_{tex}}{2}]$
11. if u occurs within veinBounds
12. return 1
13. end if
14. end if
15. return 0
16. end function

$O(\log n)$. Implemented as a shader in a ray tracing system, the venation algorithm is parallelizable and multi-resolution, making it suitable for multi-host rendering with arbitrary levels of detail generated on the fly. Supersampling of veins is often required to prevent aliasing artifacts, especially for dense venation patterns that recede into the distance.

The daylily leaves in Figure 6.11 have been rendered with non-branching parallel veins, using slightly wavy B-spline paths to keep the veins from appearing unnaturally straight. Translucent outlines have been added around the rims. The shade tree used for a single leaf is shown in Figure 6.9. The parameters for outline width, vein number, and vein width

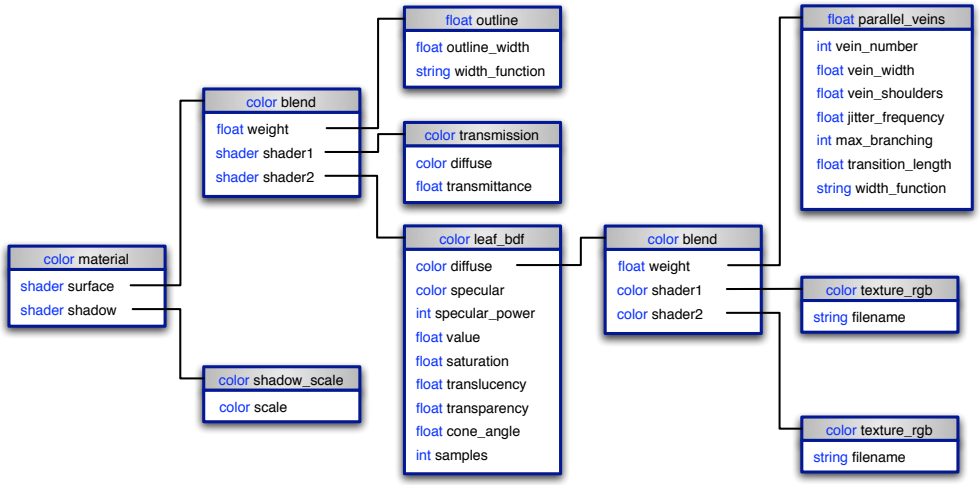

Figure 6.9: Shade tree used to render a daylily leaf.

Material(*outlineWidth*, *veinNumber*, *veinWidth*): 1 ⟶
  @Mt("material", "%m", "%m")
    @Ms("blend", "%m", "%m", "%m")
      @Ms("outline", *outlineWidth*, "leafWidth.func")
      @Ms("transmission", 0.6,0.94,0.1, 0.5)
      @Ms("leaf_bdf", "%m", "%s", 2, 0.9, 0.9, 0.7, 0.2, 10, 4)
        @Ms("blend", "%m", "%m", "%m")
          @Ms("parallel_veins", *veinNumber*, *veinWidth*, 1.6, 20, 0, 0, "leafWidth.func")
          @Ms("texture_rgb", "veins.png")
          @Ms("texture_rgb", "leafBlade.png")
  @Ms("shadow_scale", 0.5,0.5,0.5)

Figure 6.10: A production for setting the material properties of a daylily leaf. The material modules mirror the shade tree in Figure 6.9.

---

differ for every leaf, and are set via material modules in an L-system production, shown in Figure 6.10. Similarly, each of the leaves on the hyacinth in Figure 6.12 has a unique parallel vein pattern with branching. The veins fade away toward the tips of the leaves. Both the hyacinth and daylily veins were supersampled using 20 sample rays per pixel.

The parallel vein shader has several limitations. As its name implies, it is not a general venation shader, and does not produce pinnate or other non-parallel patterns. The shader does not generate areoles, making it impractical for close-up views. Finally, it is not biologically based and is not suited for simulating vein growth.

Figure 6.11: Daylily leaves.

Figure 6.12: Hyacinth

6.2.4 Particle Vein Systems

A much larger variety of vein patterns has been achieved in previous research through the use of particle systems. The changing state of particle systems over time has been used to simulate physiological processes that drive the formation of veins. Rodkaew *et al. [85]* modeled veins by spreading particles across a leaf blade. During simulation, the particles migrate toward the base of the blade, but at the same time are attracted to each other, forming branching paths that resemble primary and secondary veins. Runions *et al.* [88], taking inspiration from the plant hormone *auxin,* adopted a biologically-based approach to vein formation. Initial vein nodes placed at the base of a leaf grow toward sources of auxin distributed in the leaf blade. The formation of new veins reciprocally affects the placement of new sources of auxin. Over a period of time, this feedback loop results in intricate vein patterns.

While the patterns produced by Runions are procedurally generated, the algorithm does not permit point sampling in texture space without first having generated the entire texture. Unlike the parallel venation algorithm, the textures cannot be generated on the fly and their resolution must be decided upon prior to rendering. To use a venation pattern for rendering, the pre-generated texture must be loaded from a file or memory, processed in an image editor, and texture-mapped onto a surface. Five unique vein textures have been prepared in this way for the leaves on the backlit twig in Figure 6.13. High order venation is visible in the petals of the trillium flower in Figure 6.14. Bump mapping has been used to simulate the troughs formed by the veins. Veins on the front sides of petals are usually indented into the surface [65, 101], so a negative scaling value for the height of the bumps has been used. Appendix A describes in detail how to prepare textures and bump maps from the raw venation patterns generated by Runions' method.

Figure 6.13: Poplar leaves.

Figure 6.14: Trillium flower

Chapter 7

Plant Hairs

Hairs are a common element of many different plants. Leaves, shoots, and stems covered in hair must be properly modeled and rendered to generate photorealistic plants [24]. This chapter presents a novel method of generating hairy plants from L-systems[1].

7.1 Background

From a biological perspective, plant hairs are representative of *trichomes*, which also include such structures as scales, warts, and spines [93]. The appearance of trichomes varies from the pronounced scales covering young fern fronds to the fine hairs covering some leaves. These fine hairs are often perceived as "fuzz", and give rise to a characteristic soft glow around backlit surfaces, as illustrated in Figure 7.1. This phenomenon has been termed *asperity scattering* [46].

The mechanisms of trichome distribution on their underlying surfaces are an interesting problem in developmental biology, and have recently been studied from a molecular perspective (*e.g.* [51, 89]). Trichome placement is controlled by a signaling mechanism that prevents the formation of new organs too close to each other, and in this respect it is related to the placement of organs in phyllotactic patterns around plant stems [51]. Functionally, plant hairs and related structures play a variety of roles. For example, they may shade the plant surface from excessive exposure to sunlight, decrease the loss of water through transpiration, or ward off hungry insects or herbivores [93].

Modeling of hairs has been extensively investigated in the context of human hair and animal fur. Kajiya and Kay [41] approached fur rendering using texels, three dimensional

[1]This chapter is an edited version of the work presented in [24].

Figure 7.1: Fuzz on the leaves of Nankin cherry boughs glows brilliantly when illuminated from the rear.

---

arrays of parameters describing visual properties of the fur. Goldman [28] proposed a probabilistic method for rendering fur from a distance. The texel-based and probabilistic approaches make it possible to synthesize images of furry objects while keeping the geometry simple, but they provide only a limited control over the individual hairs. In contrast, hairs modeled as individual geometric objects allow for better interactive [15] and physically-based [2] control of individual strands. These strands can be grouped together and controlled as tufts or wisps [64, 102, 45] for performance reasons. The trade-off between level of hair representation and final appearance is further exemplified by the work of Lengyel *et al.* [50].

An important aspect of the appearance of hair and fur is the modulation of a hair's characteristics according to its position on the underlying surface. To this end, Miller [61] aligned the orientation of individual hairs according to the texture coordinates of the mesh. Gelder and Wilhelms [25] recognized the need to control fur properties of animals according to the orientation of body segments. They employed orientation vectors for various limbs,

but encountered difficulties describing orientation in areas such as the head and thoracic region. Lengyel *et al.* [50] oriented fur according to vector fields placed on meshes, and made use of an interactive combing tool to further style fur according to the modeler's taste. Fleisher *et al.* [20] explored the problem of positioning and orienting small elements ('cellular particles') across surfaces of different topologies. They described a number of strategies to tackle the problem, and illustrated their techniques by covering surfaces with scales and thorns.

Fowler *et al.* [22] proposed the first method aimed at placing elements visually related to hairs on the surfaces of plants. This method exploited phyllotactic patterns to position and orient spines on cacti and achenes (fruits) on the receptacle of goatsbeard.

The modeling of plant hairs must take into consideration several phenomena. Properties of plant hairs may vary continuously between different locations on a plant and developmental stages of plant organs. For example, hair density may be greater in young leaves, and drop off as the leaves become older. Fully mature leaves often lose all the hairs on their front and back surfaces, but maintain hairs along their edges. Hairs may be aligned in specific directions, depending on their position. Hairs on opposite sides of the same surface may be different from each other. In addition, there is much diversity in the shape of individual hairs: given any patch of hairy surface, it is common to see a mixture of hairs that are straight and curly, or long and short.

To account for these phenomena, we propose to model plants with hairs using a method with the following characteristics:

- **Geometric representation of hairs**. Individual hairs are specified as generalized cylinders, which are simplified to connected line segments during interactive modeling. This makes it possible to control the shape of hairs and their distribution across a surface in fine detail. This geometric approach is computationally efficient (e.g. plants with hairs can be previewed at interactive rates), because the density of hairs

on plants is typically low in comparison to human hair or animal fur. In addition, fewer line segments are required since plant hairs are often relatively short.

- **The use of positional information**. Many aspects of plant architecture can conveniently be characterized using functions of position along plant axes [82]. This technique is extended to plant hairs, so that hair parameters along the length and breadth of plant organs may be changed.

- **The framework of L-systems with turtle interpretation**. In addition to being a general method for modeling plant architecture, L-systems lend themselves well to the local control of hair attributes such as length, radius, curvature, and density of placement. L-system modules are used for this purpose. The turtle used to interpret L-system strings also provides a convenient frame of reference [82] for orienting hairs along plant organs such as stems, leaves, and petals.

7.2 Hair generation

The process of hair generation involves several steps. First, the hair distribution on the underlying surface is determined. Individual hairs must then be modeled, and an instance of a pre-determined hair placed at every attachment point.

7.2.1 Distribution of the attachment points

In the extensively studied case of trichome distribution on the leaves of *Arabidopsis thaliana*, the individual trichomes are spaced in a semi-regular manner, preserving a minimum distance from each other. The underlying morphogenetic process is believed to be of the reaction-diffusion type [51]. Instead of simulating this process, we approximate its outcome as a Poisson-disk pattern generated using the point diffusion algorithm proposed by Mitchell [63]. Comparisons of images indicate that trichome distribution patterns (shown,

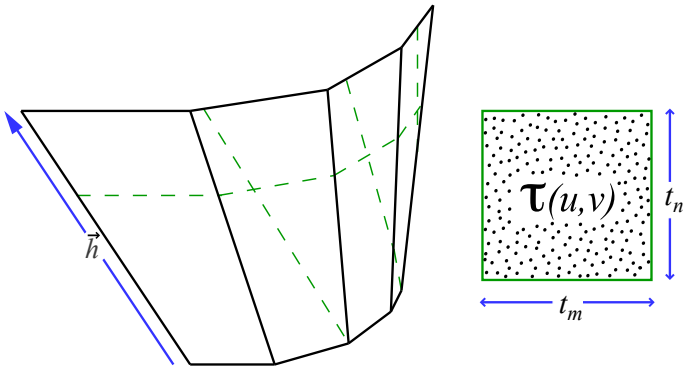

Figure 7.2: The point-diffusion texture is mapped onto the generalized cylinder segment (unfolded, curling into the page) in scan-line fashion, starting at the lower left corner and ending at the upper right corner. The mapping of the $t_m \times t_n$ texture is indicated by the dashed lines. Density of the hair is controlled by scaling the texture according to positional information.

---

for example, in [51]) are visually indistinguishable from Poisson-disk patterns (as illustrated in [63]).

Point diffusion can be viewed as a texture generation algorithm that computes a texture value (on or off) and a diffusion value at every grid element. This computation is based on previously computed diffusion values stored in a neighborhood of four adjacent elements, one to the immediate left and three in the row above. Point diffusion can be applied in two ways for distributing hairs: on-the-fly or using texture mapping. The former approach involves continuously generating the distribution pattern as the surfaces are produced. The resulting seamless pattern is ideal for offline rendering purposes, but too slow to compute during interactive modeling. We therefore preferably use the texture mapping method, whereby a single point-diffusion texture is repeatedly tiled along the surface of the plant organ. As the neighborhood used to compute the points in Mitchell's algorithm wraps around the vertical edges of the texture, vertical seams are barely visible. Horizontal seams are more conspicuous; in practice, however, once hairs have been placed and oriented, the seams are not noticeable.

The point-diffusion texture is a function $\tau(u, v) \rightarrow \{0, 1\}$, where a returned value of 1

indicates an attachment point for a hair. We have found that a texture of size 100×100 results in visually acceptable hair distribution patterns. The texture-mapping technique is illustrated in Figure 7.2. Although it introduces distortions (shear of the texture) when applied to generalized cylinders with a rapidly changing circumference or width, we have found the resulting artifacts visually negligible.

7.2.2 Hair modeling and placement

Hairs on a single plant come in many different shapes and sizes. While it is not feasible to model the shape of every hair individually, it is possible to capture the overall diversity of a hairy surface by modeling several different *template hairs* and instancing them multiple times. During this research, hairs were modeled as curved generalized cylinders constructed using simple L-systems (Figure 7.3). These hair L-systems are independent from the L-system used to generate the whole plant. We control the hair curvature with functions for tilt, twist, and pitch to rotate the turtle along its up, left, and heading vectors, respectively [82]. The number of segments used to approximate each hair depends on its curvature: relatively straight hairs can be reasonably modeled with three turtle steps, while twisted hairs may require seven or more steps. The number of individual hairs to model depends on the nature of the plant's hairy surface: for most of the models in this chapter, three to five different hairs properly capture the varied appearance of a hairy surface.

A hair is stored as a sequence of vertices describing the position of the turtle at every step. Whenever a hair is instanced, its vertices are connected together. During real-time rendering in CPFG, the vertices are connected by antialiased line segments, which are stored in a display list to improve performance. During high-quality offline rendering, the vertices are joined by cylindrical primitives. Each hair is assumed to have a constant radius.

When placing a hair on the front or back side of a generalized cylinder, we set the hair's orientation by aligning the axis of its first segment with the *hair direction vector*

Figure 7.3: Template hairs modeled as generalized cylinders generated by L-systems.

$\vec{d}$. By default, hair direction vectors are aligned with the surface's shading normals $\vec{n}$, so that hairs have the appearance of emerging perpendicularly to the surface of the plant. In the same way that shading normals are computed by linearly interpolating between the four vertex normals of a face, hair direction vectors are computed by linearly interpolating between the four *hair vertex vectors* of a face.

An open generalized cylinder also includes a specification of *hair edge vectors* for the outer edges of the first and last face. A hair edge vector is defined by the cross product of the normalized height vector $\vec{h}$ (Figure 7.2) and the shading normal $\vec{n}$, so that it points away from the cylinder segment. By default, hair direction vectors for edge hairs are aligned with the hair edge vectors.

During hair placement, we transform the vertices of the hair into the local coordinate frame formed by the shading normal $\vec{n}$, the vector $\vec{n} \times \vec{h}$, and a tangential vector $\vec{n} \times (\vec{n} \times \vec{h})$. This default hair orientation can be modified as needed (Section 7.3.3).

Collisions between hair and surface are currently not accounted for. These collisions are a likely occurrence, for example, if the hair direction vector for a curly hair is nearly tangential to the surface.

HAIR MODULE	PURPOSE
@Hf(*bool*)	enable/disable hairs on front side
@Hb(*bool*)	enable/disable hairs on back side
@He(*bool*)	enable/disable hairs along edges
@Hd($value, \{rng, fun, loc\}$)	specify density
@Hl($value, \{rng, fun, loc\}$)	specify length
@Hr($value, \{rng, fun, loc\}$)	specify radius
@Hi($value, \{rng, fun, loc\}$)	specify angle of incline
@Ht($value, \{rng, fun, loc\}$)	specify twist angle
@Hw($value, \{rng, fun, loc\}$)	specify wrapping angle
@Hp($P_1, \ldots, P_n, \{loc\}$)	specify placement probabilities
@Hm	use current material for hair rendering

Table 7.1: L-system modules for specifying hair attributes. Module parameters are explained in the text.

7.3 Control of Hair Parameters

Table 7.1 displays a set of modules for controlling hair properties within the L-system of the plant model. The module names follow the convention used by other modules in CPFG, but can be adapted for any L-system software. The basic modules for turning hair on and off accept one boolean parameter. These modules are: @Hf for hairs on the front surface, @Hb for hairs on the back surface, and @He for edge hairs. The remaining modules accept additional parameters.

The optional parameter *loc* sets the property for only those hairs in a particular location - front, back, or edge; ignoring this parameter results in the property being set for all hair types. The properties of individual hairs can be varied by specifying the *rng* parameter. This adds a random offset to the value of the property, such that the resulting value lies within the range $value \pm rng$. We also allow the specification of a *modulating function*. This function modifies the property value around the girth of a cylinder segment. The module parameter *fun* is the index of this function.

Properties may be modified after every turtle step. In the simplest case, properties are kept constant for all hairs on a generalized cylinder segment. If the step sizes are sufficiently

Algorithm 5 This L-system describes the change in hair properties for length,incline, and density along the length of a generalized cylinder. The probability of two types of hairs is also being set at everystep, and changes as we move along the cylinder (the straight hairs become more likely near the right end).The resulting image is displayed in Figure 7.4.

1. #define l 10 /* length of axis */
2. #define $\Delta s1$ /* turtle step */
3. Axiom: @Gs @Hf(1) B(0)
4. B(s): $s \leq l$
5. {
6. $relativeDistance = s/l$;
7. $len = \text{func}(1, relativeDistance)$;
8. $inc = \text{func}(2, relativeDistance)$;
9. $den = \text{func}(3, relativeDistance)$;
10. } $\longrightarrow$
11. @Hl(len) @Hi(inc) @Hd(den)
12. @Hp($relativeDistance, 1 - relativeDistance$)
13. f(Δs) @Gc B($s + \Delta s$)
14. B(s): $s \geq l \longrightarrow @Ge$

small, the sudden transition of properties from segment to segment is nearly invisible, but if the step sizes increase, visual discontinuities may become apparent. To eliminate this artifact, properties may be interpolated across segments.

Algorithm 5 presents a sample L-system used to generate the cylinder pictured in Figure 7.4. We set the total length and step size in lines 1 and 2, and begin the generalized cylinder with module $@Gs$ in the axiom of line 3. The module $@Hf$ turns on the hairs. The production B repeatedly advances the turtle and draws a generalized cylinder segment

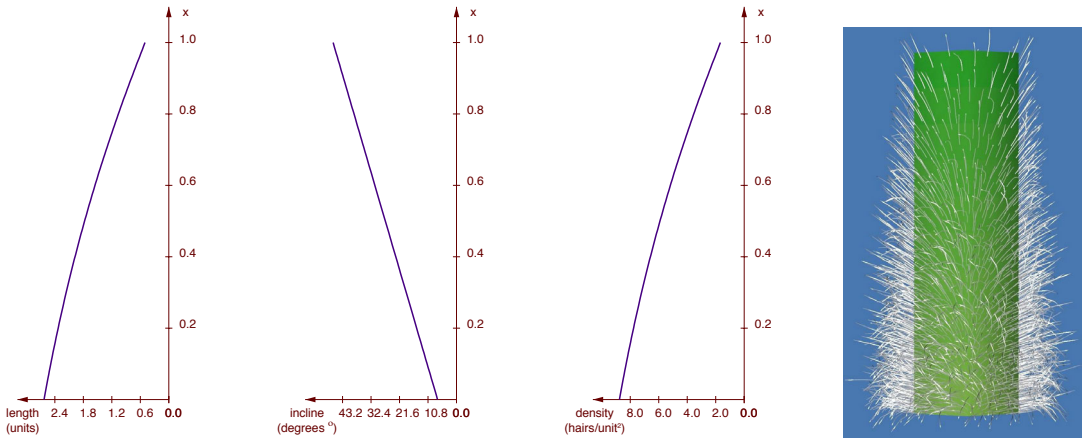

(a) (b) (c) (d)

Figure 7.4: Hair parameters for (a) length, (b) incline, and (c) density are modified according to relative position x along the generalized cylinder (d). The distribution of different types of hairs is also altered, as curly hairs near the base give way to straight hairs near the top.

@Gc (line 13) as long as the current position is less than the total axis length (line 4). For every step, we calculate the relative distance traveled by the turtle (line 6). In lines 7-9, parameters for length, incline, and density are computed as a functions of relative distance. The L-system modules in line 11 assign these properties to the hair being rendered. The actual hair shapes are selected at random from two previously defined template hairs, with the probabilities set in line 12. In this example, the first hair type is straight and it occurs with increasing probability as we move upward along the cylinder. The second hair type, a curly hair, occurs frequently at the base of the cylinder but gradually disappears toward the top.

The control of hair attributes is discussed in more detail below.

7.3.1 Density

Density is adjusted with the module @Hd. While each generalized cylinder segment is associated with a single density value, the actual density of hairs may be non-uniform if the segment's width or curvature change. In particular, the density of hairs along the inner arc of a bending cylinder will be higher than the density of hairs along the outer arc. This

behavior is consistent with our observations of hair densities along bent stems of oriental poppies.

7.3.2 Size

The relative length of a hair is adjusted with the module @Hl. Its parameter controls the hair geometry by scaling the vertex positions prior to placement. Some hairy surfaces consist of both short and long hairs mixed together. In the simplest case, we can randomize the length of the individual hairs by passing a *rng* parameter. Alternatively, we can model several template hairs with different sizes and place them together on the surface. The radius for the hair is specified by the module @Hr.

7.3.3 Orientation

Hairs do not always grow perpendicularly to a surface, but can potentially be oriented in any direction. Hair orientation can be modified with three degrees of freedom through the use of three orientation modules. For surface hairs, these modules indicate the rotation of a hair direction vector around three axes: the *twist axis* $\vec{d}$ (the hair direction vector itself), the *incline axis* $\vec{n} \times \vec{h}$, and the *wrapping axis* $\vec{n} \times (\vec{n} \times \vec{h})$. (These definitions are slightly modified in the case of edge hairs.) Since hair direction vectors are calculated via interpolation between hair vertex vectors, we simply reorient the hair vertex vectors at the four corners of every face.

The module @Ht indicates the *twist angle* and rotates the hair around the twist axis. Similarly, the module @Hi indicates the *incline angle* and rotates the hair around the incline axis, and the module @Hw indicates the *wrapping angle* and rotates the hair around the wrapping axis. This last rotation is particularly useful when modeling hairy leaves, on which it is commonly observed that hairs running close to the axis are approximately perpendicular to the leaf surface, but hairs near the edges tend to wrap around to the other

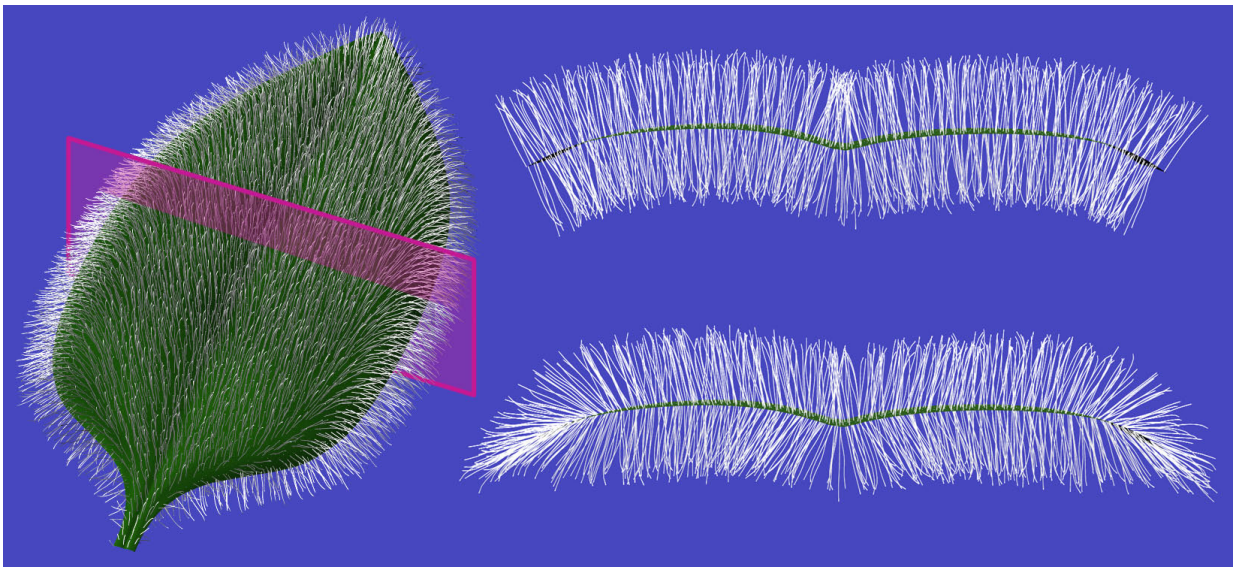

Figure 7.5: Cross-sectional view of a leaf. No hair wrapping was specified in the top cross-section. In the lower cross-section, a profile function specified by a hair-wrapping module causes hairs to gradually tilt toward the leaf edges.

side (Figure 7.5). Hence the wrapping angle is often associated with a modulating function that increases the amount of wrap as we move toward the edges of an open generalized cylinder.

As with most other properties, the orientation angles can be randomized to create hairy surfaces with a disheveled appearance. The hairs in the plant models presented in Section 7.4, for example, have a randomized twist angle.

7.3.4 Placement probability

After modeling several template hairs, we must be able to describe in what proportions they are to be distributed across the surface. The *placement probability* indicates the probability that a particular hair will be placed at a given attachment point (Figure 7.6). Given that we have modeled n hairs, the module @Hp accepts n parameters that set the placement probability for each hair.

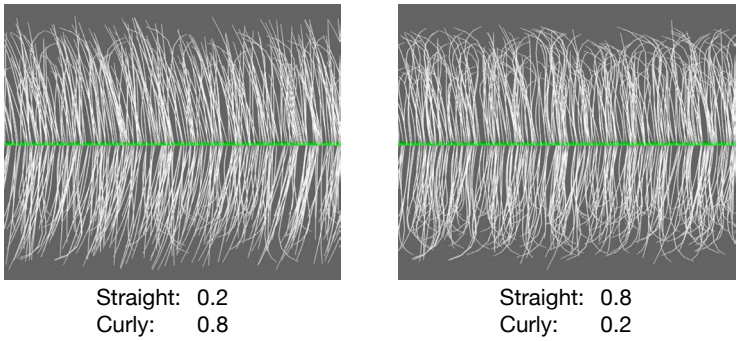

Figure 7.6: The distribution of template hairs can be controlled by assigning placement probability values. In the left image, straight hairs dominate, while in the right image, curly hairs dominate.

7.3.5 Hair Material

Material modules were introduced in Section 4.4 as a method of specifying materials for the surface of a plant. Hairs growing from the surface typically have very different material properties than the surface, so it is necessary to specify hair materials separately. The module $@Hm$ uses the material from the last material module for the purpose of shading hairs. Hairs continue to be shaded with this same material until the next occurrence of $@Hm$.

7.4 Results

This section presents several plant models that display different types of hairs. All the images were rendered using a Monte Carlo ray-tracer capable of simulating translucency and rendering hairs. The plants are visualized against solid backgrounds to better emphasize the appearance of the hairs. Hair shading is achieved with a slightly modified Kajiya model [41] that accounts for backscattering (light scattered back in the general direction of the light source), similar to the model proposed by Goldman [28]. Each model is illuminated with a single spherical light source and a hemispherical skylight.

The leaves and branches of Nankin cherries are covered in a velvety fuzz that is barely visible under normal frontlighting. Under the influence of direct backlighting, however, the

Figure 7.7: Nankin cherry branches with and without hairs, illuminated with backlight. Comparison shows the dramatic effect resulting from the inclusion of hairs in the model.

---

fuzz produces an unmistakable halo effect, as demonstrated by the photograph in Figure 7.1. Figure 7.7 simulates this effect through the use of surface hairs for the branches and edge hairs for the leaves. The image was rendered with approximately one million tiny hairs. The venation patterns were procedurally generated using the method by Runions *et al.* [88] (see Section 6.2.4) and and texture-mapped onto the leaves. Bump mapping

Figure 7.8: A photograph and a model of fern croziers.

lends the veins a sense of depth, while diffuse transmission of light is used to simulate the translucency in the leaves.

In contrast to the delicate hairs of the Nankin cherry, the fern croziers shown in Figure 7.8 are characterized by relatively large scales. The model captures changes in the length and density of scales along and around the stem.

Oriental poppies are covered in pronounced white hairs that resemble bristles but are soft to the touch. New leaves growing at the tips of fronds have a very dense covering of hairs, but the density decreases as the leaves age. At a certain point, the leaves lose all their front and back hairs, but retain edge hairs (see Figure 7.9). A fully grown (but not yet flowering) oriental poppy, with approximately 120,000 hairs, is displayed in Figure 7.10. The hair length from the base to the tip of a frond has been gradually decreased, and shorter hairs have been used for the backside of leaves. A hair wrapping function around

the leaves has also been used. While a mixture of straight and curved hairs were used for most of the plant, the placement probability for straight hairs on the bud was set to 1, and the hairs were tilted such that they became almost tangent to the surface of the bud.

In the introduction for thesis, the wild crocus (Figure 1.1) was presented as a modeling and rendering challenge, not only for its wispy hairs, but also for the fuzzy translucency and subtle venation patterns of its violet sepals. A synthetic model of the crocus containing 65,000 hairs is shown in Figure 7.11. Hair length and orientation have been varied along the surface of the sepals and finger-like leaves. Three different template hairs have been used for the model. Fuzzy translucency and procedurally generated parallel veins have been added to the sepals. The gradual browning of the leaves toward their tips is achieved by altering color parameters with material modules. Indirect lighting provided by the skylight produces subtle variations in illumination, especially where the leaves join the stem. In short, the rendered crocus is a culmination of most of the techniques presented in this research.

Figure 7.9: Comparison of a real and rendered oriental poppy frond. New leaves are covered in dense surface hairs, which fall off as the leaves age. However, edge hairs are retained.

Figure 7.10: Oriental poppy

Figure 7.11: Prairie crocus

Chapter 8

Conclusions and Future Work

This research has focused on improving the realism of plants generated with L-systems. Several approaches were taken toward this goal. A method of incorporating dynamic material specifications in L-systems has been proposed, making it possible to use material modules to generate plant models with a large variety of surface appearances. Global illumination and shading of plant surfaces, with a particular emphasis on translucency, have been discussed, taking into account observed light interactions with real leaves and petals. The fitting of textures onto generalized cylinder surfaces generated by L-systems has made it possible to map surface features onto leaves and petals. This research presented procedural methods for generating translucent outlines and venation patterns, whose parameters can be specified in the L-system with material modules. Finally, a method for generating hairs on plants was presented. Local hair parameters can be controlled using modules, in conjunction with orientation information inherent to L-systems.

The results of these approaches have contributed to increased realism in the field of plant rendering, demonstrated through the inclusion of numerous state-of-the-art renderings throughout this thesis. Improving the appearance of plants generated with L-systems is an incremental process, and there are many topics that require further exploration as part of future work:

- **Implementation of material modules in L+C.** Material modules implemented in CPFG often require long parameter lists, making it difficult to determine which value is associated with which appearance parameter. Furthermore, the ordering of the parameters lists is rigid, and must conform to the order in which the parameters are listed in the corresponding shader definition. The L+C modeling language [42] is

a formalism for expressing L-systems based on the C programming language. Using this language, it would be possible to express materials using C data structures, or *structs*, whose typed data elements would represent appearance parameters. By linking together structs into a shade tree, the entire tree could then be passed as a single parameter to a material module.

- **Real-time dynamic specification of materials.** Rendering libraries such as OpenGL are increasingly making use of real-time shaders that allow materials to be created and selected on the fly. While our discussion has focused predominantly on use of material modules for offline rendering systems, they could also be used, for example, to alternate between a real-time translucency shader for tissues and a hair shader for fuzz as a user is interactively rotating a plant model.

- **Subsurface scattering rendering techniques**. Donner and Jensen [17] recently presented a BDF that uses an efficient multiple dipole approximation to simulate scattering in thin surfaces with multiple layers, such as leaves. Scattering in thicker, volumetric organs such as soft stems would further benefit from a full BSSDF treatment. It would be interesting to further explore these advanced rendering techniques on full plant models.

- **Enhanced parallel venation shader.** The shader implemented for this research does not simulate the fusing of veins commonly observed at the tips of monocot leaves [65]. This functionality could be added by changing the vein representation from binary trees to cyclic graphs.

- **Multiscale modeling based on biological simulations**. Our approach to modeling plants with hair is purely phenomenological: we use a Poisson distribution to position hairs on their supporting surfaces, and reproduce the shape of individual hairs according to their observed appearance. It may be interesting, at least from a

biological perspective, to simulate the underlying morphogenetic processes according to current biological theories and hypotheses.

Appendix A

A Recipe for Leaf Venation Textures in Photoshop

The preparation of textures is an important step in creating believable renderings. Carefully prepared surface textures, along with associated bump maps and specular maps, can transform even simple geometric surfaces into vibrant leaves and petals during the rendering stage [96]. While synthetic generation of textures produces increasingly intricate results, the resulting image often requires a scrutinizing eye and helping hand from a user to create the desired final appearance. A good example is the synthetic generation of venation patterns [88]. While the patterns closely match vein systems found in nature, they must still be manually inserted into a leaf blade texture and processed for bump mapping before the final texture can be passed to the renderer.

This appendix describes the preparation of the trillium vein texture and bump map used for Figure 6.14. It is often necessary to prepare several texture files with slightly different vein patterns, in order to produce a non-uniform appearance of leaves and petals. With the help of layers, one of our goals is to make it easy to reuse the same vein image to generate multiple textures. The description is aimed at users of Adobe Photoshop [98], although in practise any advanced image editing program that supports layers, paths, channels, and noise filters may be used. Menu commands are written as *Menu* > *Item*, or where submenu items are involved, as *Menu* > *Submenu* > *Item*.

Initial Processing

The unprocessed venation pattern starts out as a black and white image (Figure A.1). Veins are white on a black background. Copy the image into a new document and save it with the name *Venation*. Veins created by particle systems may appear somewhat ragged,

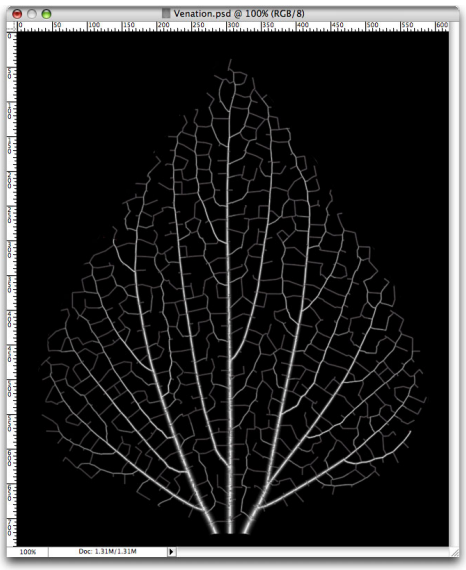

Figure A.1: The initial vein pattern used to generate the petal texture and bump map.

---

especially if the lines are not antialiased. To soften the veins, apply a Gaussian Blur *(Filter > Blur > Gaussian Blur)* using a blur radius from one to five pixels, depending on the amount of smoothing desired.

Now we must define the outline of the leaf or petal. Using the Pen tool, create a path that encloses the venation pattern. In the Paths window, name the path *Outline* and load the path as a selection. The venation pattern should now be enclosed by a marquee. Copy the pattern to the clipboard.

Petal Texture

To prepare the image texture, start by creating a new document. In the New Document dialog box, Photoshop suggests a width and height identical to the bounds of the pattern in the clipboard. Increase the document size by at least ten percent in both dimensions. Since we wish to reuse this document for several venation patterns, we must leave a bit of extra space to accommodate patterns of varying sizes. Name the document *Petal Texture*.

Next we must choose the colors to be used for the blade of the petal. While it might be tempting to use a single reddish color, plant surfaces are usually a mix of several shades of

color. For the trillium, blending together two shades of maroon produces a more believable surface. In the *Layers* window, set the name of the existing layer to *Blade Color 1.* Prepare the first shade of maroon (e.g. *RGB 180, 8, 57*) and fill the entire layer with the color. Create another layer named *Blade Color 2*, and fill it with a second shade of maroon (e.g. *RGB 108, 2, 32*).

Now create a layer mask for *Blade Color* 2. The idea is to fill the mask with a black and white noise texture. Black areas hide the maroon in the top layer *(Blade Color* 2), white areas hide the maroon in the lower layer (*Blade Color 1*), and grey areas blend together the colors to varying degrees.

In the *Channels* window, make your mask visible and hide all other channels. Set the foreground and background colours to black and white respectively. Generate a billowy effect by choosing *Filter* > *Render* > *Clouds*. Add specks by choosing *Filter* > *Noise* > *Add Noise*. For noise parameters, use 40% for amount and select the uniform distribution and monochromatic options. Soften the noise with a Gaussian Blur, using a pixel radius of about 3. The mask should now appear as in Figure A.2-a. Turn on the RGB channel to see the mask in action (Figure A.2b).

Finally, we need to add the veins. Create a new layer with the title *Vein Color.* Pick a deep shade of maroon (*RGB 35, 0, 6* works well) to make the veins stand out, and fill the layer. We want the *Vein Color* layer to show through the vein patterns, and the *Blade Color* layers to appear between the veins. To achieve this, create a new layer mask and copy the vein pattern from the *Venation* document. In the *Channels* window, paste the veins into the *Vein Color Mask* channel. Switching back to the *Layers* window, the stack of layers and layer masks should appear as in Figure A.4a.

Select *Edit* > *Copy Merged* to copy all visible layers together, and paste the final image texture into a new document (Figure A.5a).

By reusing the *Petal Texture* document as a kind of template, creating new vein textures

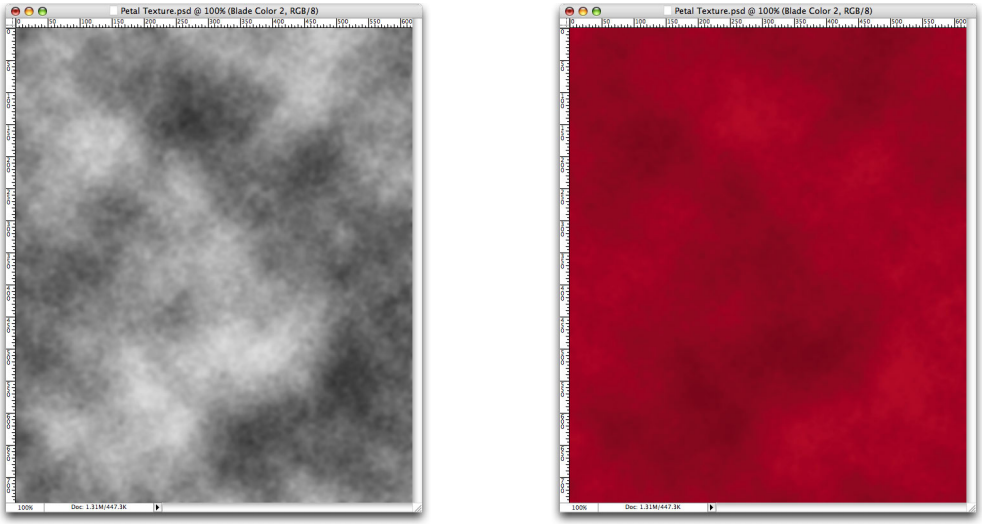

(a) (b)

Figure A.2: The layer mask in (a) is used to blend together petal colors, resulting in image (b).

---

is relatively easy. New colors for the blade and veins can be added to each of the three layers. (For even more color variation, choose two different foreground and background colors for every layer and fill each layer using the Clouds filter.) The texture for blending blade colors can be easily regenerated in the layer mask. Most importantly, a new vein pattern can be pasted into the vein mask to generate a striking new variation of the texture.

Bump Map

In order to make the veins on the the trillium petal stand out, our bump map must emphasize the veins and their immediate surroundings. Primary and secondary veins are dominant, forming troughs that run longitudinally along the petal. Tertiary veins traversing the ridges between these troughs are also bump mapped, but to a lesser extent.

Begin by copying the outline selection of the venation pattern in the *Venation* document. Create a new document with the name *Bump Map*, using the suggested dimensions. Create two layer sets (*Layer* > *New* > *Layer Set*), and name the lower set *Tertiary* and the upper set *Primary.* Add two new layers to the *Tertiary* set. Fill the lower layer with black, and

paste the venation pattern into the upper layer. Repeat for the *Primary* set: add two new layers, filled with solid black and the venation pattern, respectively. At this point, the *Layers* window should appear as in Figure A.4b. Command-click or Control-click on one of the venation layers to create an outline selection of the petal, and save this selection to a channel (*Select* > *Save Selection*). For now, hide the *Tertiary* set, as we will first create the bump maps for the primary and secondary veins.

Our goal is to generate gradients around the vein paths, in order to simulate the indentation of veins in the petal. Select the Magic Wand tool, and set Tolerance to a low value (below 20 is fine) and uncheck Contiguous. Click anywhere in a black region between the veins to select the entire blade, excluding veins. Press delete to remove these black regions (nothing will appear to change, as deleting black regions will only expose the black layer below). Invert the selection to capture the veins, and fill the selection with solid white.

We can now use the layer stroke effect (*Layer* > *Layer Style* > *Stroke*) to make the veins bumpy. Set *Fill Type* to *Gradient* and *Style* to *Shape Burst*. Create a new gradient to reflect the falloff from the veins to the petal blade. Adjust the size slider to set how far the falloff extends. The bump map should appear as in Figure A.4a.

Now we can turn our attention to primary and secondary veins. Make the *Primary* set visible. In order to remove the tertiary veins from the venation layer, repeatedly apply a Gaussian Blur and Levels adjustment to tighten up the veins. These operations should be performed in small increments to prevent the veins from breaking up. For example, each Gaussian Blur should not have a pixel radius greater than two. For each Levels adjustment, set the left input slider to a value between 10 and 100. Once the tertiary veins fade out completely, use the Eraser tool to remove any disjoint veins. As before, use the Magic Wand to select the black blade regions and clear them. Then invert the selection and fill the veins with white.

Apply the layer stroke effect to the primary and secondary veins. Set the size slider

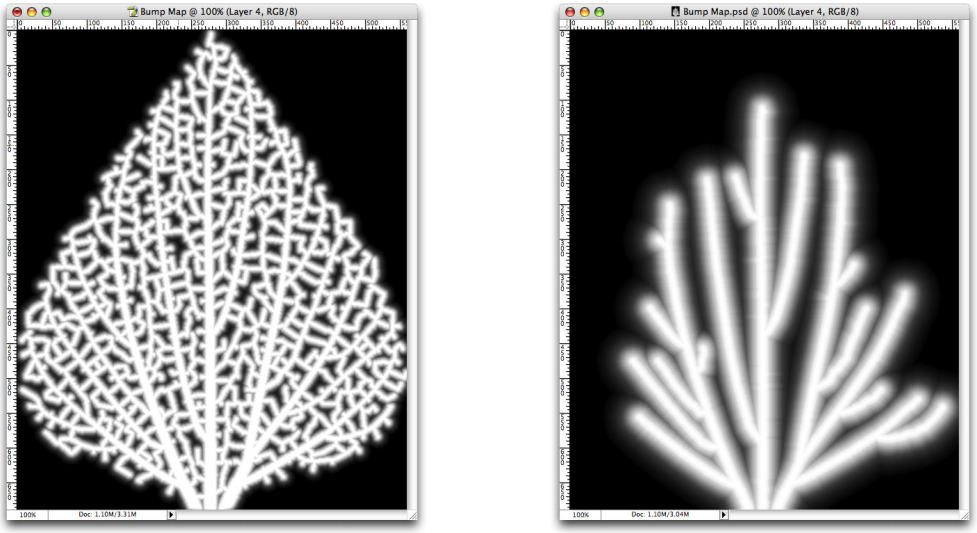

(a) (b)

Figure A.3: Bump maps for the a) tertiary veins b) primary/secondary veins

---

to a considerably larger value than the one used for tertiary veins, in order to emphasize the dominant troughs formed by the primaries and secondaries. Figure A.4b illustrates the resulting bump map.

Finally, set the opacity value of the *Primary* set to about 50%, to allow the veins from the *Tertiary* set to show through. You can continue to tweak the stroke effects in each of the layer sets until you are happy with the bump map. Load the outline selection you had saved earlier (*Select* > *Load Selection*), and copy the bump map into a new image (Figure A.5a).

Generating new bump maps tends to be more tedious than generating new image textures, because each new venation pattern must be carefully processed to extract the primary, secondary, and tertiary veins. Hence, a new bump map must be created from scratch for each venation pattern. While bump maps will not have much effect on leaves or petals that are rendered in the distance, they are definitely worth the effort to generate for close-up shots.

(a) (b)

Figure A.4: Layer and layer mask arrangements for a) the *Petal Texture* document and b) the *Bump Map* document.

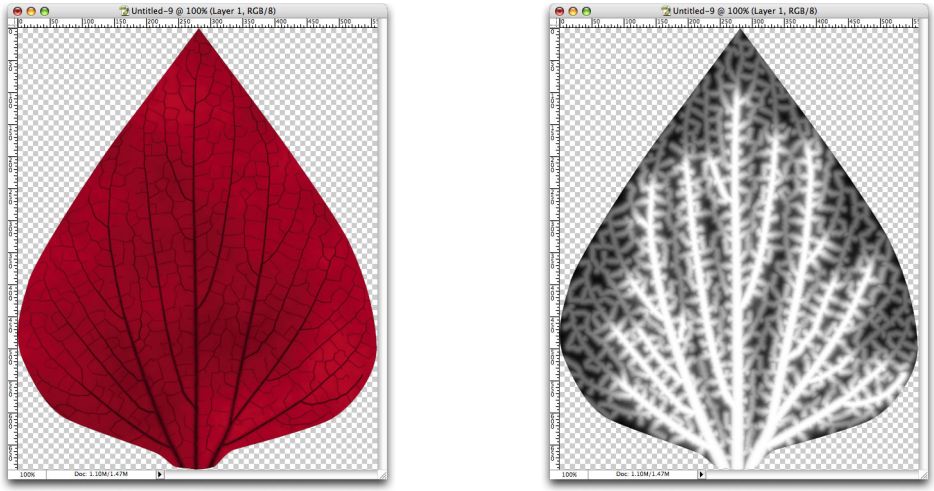

(a) (b)

Figure A.5: Final images of a) the petal texture and b) its corresponding bump map.

Additional Maps

The realism of the rendered petal can further be heightened by generating a *specularity map*, to concentrate highlights in particular areas of the blade, and a *stencil map*, to create ragged edges. These additional steps are well documented in [96].

Appendix B

Additions to cpfg

This section summarizes specific L-system modules and view file commands that have been added to CPFG during the course of this research. The section is intended to be an addendum to the existing CPFG manual [59].

Predefined Functions

The following functions query various properties of the Phong material at index i in the material table. These functions are useful for generating material module parameters based on the material table.

`ambR(`i`)`: red component of the ambient color

`ambG(`i`)`: green component of the ambient color

`ambG(`i`)`: blue component of the ambient color

`difR(`i`)`: red component of the diffuse color

`difG(`i`)`: green component of the diffuse color

`difG(`i`)`: blue component of the diffuse color

`spcR(`i`)`: red component of the specular color

`spcG(`i`)`: green component of the specular color

`spcB(`i`)`: blue component of the specular color

`coef(`i`)`: specular coefficient

Interpreted Modules

Interpreted modules are the building blocks of strings in the L-system file. Several new modules have been specified for materials and hairs.

Dynamically Specified Materials

New materials may now be specified during L-system interpretation using the following modules:

`@Mt("`*shader*`",` $value_1$`, ... ,`$value_n$`)`: The material module specifies a new material, based on the shading model *shader* and using parameters $value_n$. *shader* is the name of the shader specified as a string, and its corresponding shader description must be included in the shader file. The *value* parameters may be *int*, *float*, or *string*, depending on the parameter types specified by the shading model. *Value* parameters may also consist of material table tokens (*%a*, *%d*, *%s*, *%h*) that substitute values from the current material in the material table (see Table 4.2), or sub-material tokens (*%m*) used for building shade trees. Materials specified by material modules form the root node of a shade tree.

`@Ms("`*shader*`",` $value_1$`, ... ,`$value_n$`)`: The sub-material module specifies a new sub-material, based on the shading model *shader* and using parameters $value_n$. Sub-materials function like materials, except that they form the child nodes of a shade tree. Sub-material modules are referenced by a parent (sub)material via the sub-material token (*%m*).

Hairs

Hair modules control the appearance of hair on the surface of a generalized cylinder mesh.

`@Hf(`*bool*`)`: Enables or disables hairs on the front side of the mesh. *bool* can be `on` or `off`.

`@Hb(`*bool*`)`: Enables or disables hairs on the back side of the mesh. *bool* can be `on` or `off`.

`@He(`*bool*`)`: Enables or disables hairs along the edges of the mesh. *bool* can be `on` or `off`.

`@Hd(`$value, \{rng, fun, loc\}$`)`: Specifies the density of hairs. A value of 1 will generate a single hair on a cylinder with a width and circumference of one.

`@Hl(`$value, \{rng, fun, loc\}$`)`: Specifies the length of hairs.

`@Hr(`$value, \{rng, fun, loc\}$`)`: Specifies the radius of hairs.

`@Hi(`$value, \{rng, fun, loc\}$`)`: Specifies the incline angle of hairs along the generalized cylinder.

`@Ht(`$value, \{rng, fun, loc\}$`)`: Specifies the twist angle along the hair's axis.

`@Hw(`$value, \{rng, fun, loc\}$`)`: Specifies the wrapping angle of hairs around the generalized cylinder.

`@Hp(`$P_1, ..., P_n, \{loc\}$`)`: Specifies the placement probability for each template hair.

The optional parameters are explained below:

loc Sets the property for hairs in a particular location of the surface: front (0), back (1), or edge (2)

fun Index to a modulating function that modifies *value* around the girth of a cylinder. The function is specified in the view file.

rng Specifies the maximum bounds for varying the properties of individual hairs. The property will be a random value within the range $value \pm rng$

View File

The view file contains various drawing, viewing, and rendering parameters. The following new parameters may now be included in view file:

Textures

Two new subcommands for specifying texture files exist:

`I:` When present, makes the texture file invisible during OpenGL rendering. This is useful for forcing the generation of texture coordinates on a mesh without displaying a texture.

`T:` *tiles* Indicates how many times the texture should be tiled from start to tip of a generalized cylinder. If both `T:` and `R:` are specified, the last subcommand takes dominance.

`M:` *mapping* Indicates how v coordinates are mapped along a generalized cylinder. *mapping* may be `a`, for incrementing coordinates at uniformly intervals along the cylinder axis, or `s`, for placing coordinates uniformly along the cylinder surface.

Dynamically Specified Materials

`material modules:` *state* Determines whether or not to use material modules. *state* can be `on` or `off`.

`shader:` *filename* Specifies the name of the shader file containing shader descriptions. All material module parameters used in the L-system are validated against these shader descriptions.

Hairs

`hair:` $axis\_file_1[:probability_1]$ ... $axis\_file_n[:probability_n]$ Specifies the hair axis files to be used for generating hairs (Figure B.1). Each axis file may optionally be associated

n	4
$x_1\ y_1\ z_1\ radius_1$	0 0 0 1
$x_2\ y_2\ z_2\ radius_2$	0 0.2 0 0.9
$\cdots$	0 0.6 0.1 0.7
$x_n\ y_n\ z_n\ radius_n$	0 0.9 0.2 0.4

Figure B.1: Format of a hair axis file (left). n is the number of vertices that define the hair's axis. Each vertex is listed as an (x, y, z) coordinate, along with a radius scaling value. This scaling value is multiplied by the radius parameter from the @Hr module, and can be used to adjust the radius of a hair along its length. Vertices and radius scaling values are listed in order from the base to the tip of a hair. A sample hair axis file with four vertices is shown (right).

---

with a placement probability value, indicating the probability that a particular hair will occur relative to all other hairs. By default, CPFG assigns each hair a placement probability of $\frac{1}{n}$, where n is the number of hair axis files. If the sum of all placement probabilities is not 1, CPFG automatically recalculates and weights the probabilities to meet this condition.

`antialiasing`: *state* Enables or disables antialiasing of polygons or lines in OpenGL. This option is useful for making hairs appear soft. *state* can be `on` or `off`.

Bibliography

[1] H. Abelson and A. DiSessa. *Turtle Geometry: The Computer as a Medium for Exploring Mathematics*. MIT Press, Cambridge, MA, 1981.

[2] K. Anjyo, Y. Usami, and T. Kurihara. A simple method for extracting the natural beauty of hair. In *Proceedings of SIGGRAPH '92*, pages 111–120, 1992.

[3] G. B. Arfken, D. F. Griffing, D. C. Kelly, and J. Priest. *University Physics*. Harcourt Brace Jovanovich, San Diego, 2nd edition, 1989.

[4] G. Baranoski and J. Rokne. An algorithmic reflectance and transmittance model for plant tissue. *Computer Graphics Forum 16*, 16:141–150, 1997.

[5] G. Baranoski and J. Rokne. Efficiently simulating scattering of light by leaves. *The Visual Computer*, 17:491–505, 2001.

[6] R. Bartels, J. Beatty, and B. Barsky. *An introduction to splines for use in computer graphics and geometric modeling*. Morgan Kaufmann, Los Altos, CA, 1987.

[7] J. F. Blinn and M. E. Newell. Texture and reflection in computer generated images. *Communications of the ACM*, 19(10):542–547, October 1976.

[8] J. Bloomenthal. Modeling the mighty maple. In *Proceedings of SIGGRAPH '85*, pages 305–311, 1985.

[9] P. Bui-Tong. Illumination for computer generated pictures. In *Communications of the ACM*, volume 18, pages 311–317, June 1975.

[10] T. Burge. A branching cellular texture basis function. In *SIGGRAPH 2000 Technical Sketch*, 2000.

[11] E. Catmull. *A subdivision algorithm for computer display of curved surfaces.* PhD thesis, University of Utah, Salt Lake City, UT, December 1974.

[12] R. L. Cook. Shade trees. In *Proceedings of SIGGRAPH '84*, pages 223–231, 1984.

[13] R. L. Cook. Stochastic sampling in computer graphics. *ACM Transactions on Graphics*, 5(1):51–72, 1986.

[14] R. L. Cook, T. Porter, and L. Carpenter. Distributed ray tracing. In *Proceedings of SIGGRAPH '84*, pages 137–145, 1984.

[15] A. Daldegan, N. Thalmann, T. Kurihara, and D. Thalmann. An integrated system for modeling, animating and rendering hair. In *Computer Graphics Forum*, pages 211–221, 1993.

[16] P. Debevec. Image-based lighting. *IEEE Computer Graphics and Applications*, 22(2):26–34, March/April 2002.

[17] C. Donner and H. W. Jensen. Light diffusion in multi-layered translucent materials. In *Proceedings of SIGGRAPH '05*, 2005.

[18] D. Ebert, K. Musgrave, D. Peachey, K. Perlin, and S. Worley. *Texturing and Modeling: A Procedural Approach.* Academic Press, San Diego, CA, 1994.

[19] P. Federl. Vlab documentation. Website, 1999. www.algorithmicbotany.org/vlab.

[20] K. W. Fleischer, D. H. Laidlaw, B. L. Currin, and A. H. Barr. Cellular texture generation. In *Proceedings of SIGGRAPH '95*, pages 239–248, 1995.

[21] J. D. Foley, A. van Dam, S. K. Feiner, and J. F. Hughes. *Computer Graphics: Principles and Practice.* Addison-Wesley, Reading, Massachusetts, 2nd edition, 1997.

[22] D. R. Fowler, P. Prusinkiewicz, and J. Battjes. A collision-based model of spiral phyllotaxis. In *Proceedings of SIGGRAPH '92*, pages 361–368, 1992.

[23] O. Franzke and O. Deussen. Rendering plant leaves faithfully. In *Proceedings of the SIGGRAPH 2003 Conference on Sketches*, page 1, 2003.

[24] M. Fuhrer, H. W. Jensen, and P. Prusinkiewicz. Modeling hairy plants. In *Proceedings of Pacific Graphics '04*, pages 217–236, 2004.

[25] A. V. Gelder and J. Wilhelms. An interactive fur modeling technique. In *Proceedings of Graphics Interface '97*, pages 181–188, 1997.

[26] E. M. Gifford and A. S. Foster. *Morphology and Evolution of Vascular Plants.* W. H. Freeman and Company, New York, 1996.

[27] A. S. Glassner. *Principles of Digital Image Synthesis.* Morgan Kaufmann, San Francisco, 1995.

[28] D. Goldman. Fake fur rendering. In *Proceedings of SIGGRAPH '97*, pages 127–134, 1997.

[29] C. M. Goral, K. E. Torrance, D. P. Greenberg, and B. Battaile. Modeling the interaction of light between diffuse surfaces. In *Proceedings of SIGGRAPH '84*, pages 213–222, 1984.

[30] L. Grant. Diffuse and specular characteristics of leaf reflectance. *Remote Sensing Environment*, 22:309–322, 1987.

[31] J.S. Hanan. *Parametric L-systems and their application to the modelling and visualization of plants.* PhD thesis, University of Regina, June 1992.

[32] P. Hanrahan and W. Krueger. Reflection from layered surfaces due to subsurface scattering. In *Proceedings of SIGGRAPH '93*, volume 165-174, 1993.

[33] P. Hanrahan and J. Lawson. A language for shading and lighting calculations. In *Proceedings of SIGGRAPH '90*, pages 289–298, 1990.

[34] L. J. Hickey. A revised classification of the architecture of dicotyledonous leaves. In C. R. Metcalfe and L. Chalk, editors, *Anatomy of the dicotyledons*, volume 1, pages 25–39. Clarendon Press, 1979.

[35] H. W. Jensen. *Realistic Image Synthesis Using Photon Mapping*. A K Peters, Natick, Massachusetts, 2001.

[36] H. W. Jensen. Dali rendering system. Software, 2004.

[37] H. W. Jensen and J. Buhler. A rapid hierarchical rendering technique for translucent materials. In *Proceedings of SIGGRAPH '02*, pages 576–581, 2002.

[38] H. W. Jensen, S. R. Marschner, M. Levoy, and P. Hanrahan. A practical model for subsurface light transport. In *Proceedings of SIGGRAPH '01*, pages 511–518, 2001.

[39] G. H. Joblove and D. P. Greenberg. Color spaces for computer graphics. In *Proceedings of SIGGRAPH '78*, pages 20–25, 1978.

[40] J. T. Kajiya. The rendering equation. In *Proceedings of SIGGRAPH '86*, pages 143–150, 1986.

[41] J. T. Kajiya and T. L. Kay. Rendering fur with three dimensional textures. In *Proceedings of SIGGRAPH '89*, pages 271–280, 1989.

[42] R. Karwowski and P. Prusinkiewicz. Design and implementation of the l+c modeling language. *Electronic Notes in Theoretical Computer Science*, 86(2):19, 2003.

[43] R. Karwowski and P. Prusinkiewicz. The L-system-based plant-modeling environment l-studio 4.0. In *Proceedings of the 4th International Workshop on Functional-Structural Plant Models*, pages 403–405, 2004.

[44] D. S. Kay. Transparency, refraction, and ray tracing for computer synthesized images. Master's thesis, Cornell University, Ithaca, NY, January 1979.

[45] T.-Y. Kim and U. Neumann. Interactive multiresolution hair modeling and editing. In *Proceedings of SIGGRAPH '02*, pages 620–629, 2002.

[46] J. Koenderink and S. Pont. The secret of velvety skin. *Machine vision and applications*, 14:260–268, 2003.

[47] A. A. Kokhanovsky. On the determination of the refractive index of strongly absorbing particles dispersed in a non-absorbing host medium. *Journal of Physics D: Applied Physics*, 32:825–831, 1999.

[48] C. Kolb and R. Bogart. Rayshade 4.0. Open source software, 1991.

[49] S. Lefebvre and F. Neyret. Synthesizing bark. In *Proceedings of the 13th Eurographics workshop on Rendering Rendering*, pages 105–116, 2002.

[50] J. Lengyel, E. Praun, A. Finkelstein, and H. Hoppe. Real-time fur over arbitrary surfaces. In *Proceedings of the ACM Symposium on Interactive 3D Graphics*, pages 227–232, 2001.

[51] O. Leyser and S. Day. *Mechanisms in plant development*. Blackwell, Oxford, 2003.

[52] A. Lindenmayer. Mathematical models for cellular interaction in development, Parts I and II. *Journal of Theoretical Biology*, 18:280–315, 1968.

[53] R. Lu, J. J. Koenderink, and A. M. Kappers. Optical properties (bidirectional reflectance distribution functions) of velvet. *Applied Optics*, 37(25):5974–5984, 1998.

[54] K. Maritaud. *Rendu réaliste d'arbres vus de près en images de synthèse images de synthèse*. PhD thesis, University de Limoges, France, December 2003.

[55] W. R. Mark, R. S. Glanville, K. Akeley, and M. J. Kilgard. Cg: a system for programming graphics hardware in a C-like language. *ACM Transactions on Graphics*, 22(3):896–907, 2003.

[56] S. Marschner, S. Westin, E. Lafortune, and K. Torrance. Image-based BRDF measurement. *Applied Optics*, 39(16):2592–2600, 2000.

[57] W. Matusik. Homogeneous isotropic BRDFs. Realistic Materials in Computer Graphics SIGGRAPH '05 Course Notes, 2005.

[58] R. Měch. *Modeling and simulation of the interactions of plants with the environment using L-systems and their extensions.* PhD thesis, University of Calgary, October 1997.

[59] R. Měch. CPFG version 3.4 user's manual, 1998. Manuscript, Department of Computer Science, University of Calgary.

[60] R. Melville. The terminology of leaf architecture. *Taxon*, 25(5/6):549–561, 1976.

[61] G. Miller. From wire-frame to furry animals. In *Proceedings of Graphics Interface '88*, pages 138–146, 1988.

[62] G. S. Miller and C. R. Hoffman. Illumination and reflection maps: Simulated objects in simulated and real environments. In *SIGGRAPH '84 Course Notes for Advanced Computer Graphics Animation*, 1984.

[63] D. P. Mitchell. Generating antialiased images at low sampling densities. In *Proceedings of SIGGRAPH '87*, pages 65–72, 1987.

[64] M. Nakajima, S. Saruta, and H. Takahashi. Hair image generating algorithm using fractional hair model. In *Signal Processing: Image Communication 9*, pages 267–273, 1997.

[65] T. Nelson and N. Dengler. Leaf vascular pattern formation. *The Plant Cell*, 9:1121–1135, July 1997.

[66] F. E. Nicodemus, J. C. Richmond, J. J. Hsia, I. W. Ginsberg, and T. Limperis. Geometric considerations and nomenclature for reflectance. *NBS Monograph 160*, 1977.

[67] T. Nishita and E. Nakamae. Continuous tone representation of three-dimensional objects taking account of shadows and interreflection. In *Proceedings of SIGGRAPH '85*, pages 23–30, 1985.

[68] M. Olano and A. Lastra. A shading language on graphics hardware: The pixelflow shading system. In *Proceedings of SIGGRAPH '98*, pages 156–168, 1998.

[69] D. R. Peachey. Solid texturing of complex surfaces. In *Proceedings of SIGGRAPH '85*, pages 279–286, 1985.

[70] K. Perlin. An image synthezier. In *Proceedings of SIGGRAPH '85*, pages 287–296, 1985.

[71] M. Pharr. Layered media for surface shaders. Advanced RenderMan SIGGRAPH '02 Course Notes, 2002.

[72] B. T. Phong. Illumination for computer generated pictures. *Communications of the ACM*, 18(6):311–317, June 1975.

[73] A. J. Preetham, P. Shirley, and B. Smits. A practical analytic model for daylight. In *Proceedings of SIGGRAPH '99*, pages 91–100, 1999.

[74] P. Prusinkiewicz. Graphical applications of L-systems. In *Proceedings of Graphics Interface '86*, pages 247–253, 1986.

[75] P. Prusinkiewicz. Modelling and visualization of biological structures. In *Proceedings of Graphics Interface '93*, pages 128–137, May 1993.

[76] P. Prusinkiewicz, M. Hammel, and E. Mjolsness. Animation of plant development. In *Proceedings of SIGGRAPH '93*, pages 351–360, 1993.

[77] P. Prusinkiewicz and J. Hanan. Visualization of botanical structures and processes using parametric L-systems. In D. Thalmann, editor, *Scientific Visualization and Graphics Simulation*, pages 183–201, Chichester, 1990. J. Wiley Sons.

[78] P. Prusinkiewicz, J. Hanan, and R. Měch. An L-system-based Plant Modeling Language, 2000. Lecture Notes in Computer Science 1779, pages 395–410. Springer-Verlag, Berlin.

[79] P. Prusinkiewicz, M. James, and R. Měch. Synthetic topiary. In *Proceedings of SIGGRAPH '94*, pages 351–358, 1994.

[80] P. Prusinkiewicz, R. Karwowski, R. Měch, and J. Hanan. L-studio/cpfg: A software system for modeling plants. In M. Nagl, A. Schürr, and M. Münch, editors, *Applications of graph transformation with industrial relevance*, Lecture Notes in Computer Science 1779, pages 457–464. Springer-Verlag, Berlin, 2000.

[81] P. Prusinkiewicz and A. Lindenmayer. *The algorithmic beauty of plants*. Springer-Verlag, New York, 1990.

[82] P. Prusinkiewicz, L. Mündermann, R. Karwowski, and B. Lane. The use of positional information in the modeling of plants. In *Proceedings of SIGGRAPH '01*, pages 289–300, 2001.

[83] X. Qin, E. Nakamae, K. Tadamura, and Y. Nagai. Fast photo-realistic rendering of trees in daylight. *Computer Graphics Forum*, 22(3):243–252, 2003.

[84] V. Raghavan. *Developmental Biology of Flowering Plants*. Springer-Verlag, New York, 2000.

[85] Y. Rodkaew, S. Siripant, C. Lursinsap, and P. Chongstitvatana. An algorithm for generating vein images for realistic modeling of a leaf. In *Proceedings of the International Conference on Computational Mathematics and Modeling*, pages 73–78, 2002.

[86] Y. Rodkaew, S. Siripant, C. Lursinsap, P. Chongstitvatana, T. Fujimoto, and N. Chiba. Modeling leaf shapes using L-systems and genetic algorithms. In *Proceedings of NICOGRAPH '02*, pages 1–6, Japan, April 2002.

[87] R. J. Rost, D. Baldwin, and R. Rost. The OpenGL shading language. Technical Report Language Version 1.10, 3Dlabs, Inc., April 30, 2004.

[88] A. Runions, M. Fuhrer, B. Lane, A. Rolland-Lagan, P. Federl, and P. Prusinkiewicz. Modeling and visualization of leaf venation patterns. In *Proceedings of SIGGRAPH '05*, pages 702–711, 2005.

[89] A. Schnittger, U. Folkers, B. Schwab, G. Jürgens, and M. Hülskamp. Generation of a spacing pattern: The role of *TRIPTYCHON* in trichome patterning in *Arabidopsis*. *Plant Cell*, 11:1105–1116, 1999.

[90] A. L. Szilard and R. E. Quinton. An interpretation for DOL systems by computer graphics. *The Science Terrapin*, 4:8–13, 1979.

[91] N. Tatarchuk and C. Brennan. Simulation of iridescence and translucency on thin surfaces. In *ShaderX 2: Shader Programming Tips and Tricks with DirectX 9*, pages 1–11. Worldwide Publishing, 2003.

[92] K. E. Torrance and E. M. Sparrow. Theory for off-specular reflection from roughened surfaces. *Journal of Optical Society of America*, 57(9):1105–1114, 1967.

[93] J. C. Uphof. *Plant hairs*. Gebrüder Borntraeger, Berlin, 1962.

[94] S. Upstill. *The Renderman Companion*. Addison-Wesley, Reading, Massachusetts, 1990.

[95] F. R. Vance, J. R. Jowsey, J. S. McLean, and F. A. Switzer. *Wildflowers Across the Prairies*. Greystone Books, 3rd edition, 1999.

[96] F. Vitale. Surfacing: Half the battle. In *Mastering 3D Graphics: Digital Botany and Creepy Insects*, pages 147–165. John Wiley and Sons, 2000.

[97] G. J. Ward. Measuring and modeling anisotropic reflection. In *Proceedings of SIGGRAPH '92*, pages 265–272, 1992.

[98] J. Warnock and C. Geschke. Adobe Photoshop CS. Commercial Software, 2003. www.adobe.com/photoshop.

[99] T. Whitted. An improved illumination model for shaded display. *Communications of the ACM*, 23(6):343–349, June 1980.

[100] T. Whitted and D. M. Weimer. A software testbed for the development of 3D raster graphics systems. *ACM Transactions on Graphics*, pages 43–58, 1982.

[101] J. T. Woolley. Reflectance and transmittance of light by leaves. *Plant Physiology*, 47:656–662, 1971.

[102] X. D. Yang, Z. Xu, T. Wang, and J. Yang. The cluster hair model. *Graphical Models*, 62(2):85–103, 2000.